

ALDOT Research Project 931-015

Local Verification of AASHTOWare™ Pavement ME Design for Flexible Pavement

Final Report

July 2024



1. Report No.	2. Government Accession No.	3. Recipient's Catalog No.	
4. Title and Subtitle Local Verification of AASHTOWare™ Pavement ME Design for Flexible Pavement		5. Report Date July 2024	
		6. Performing Organization Code	
7. Author(s) Nam Tran, Akeem Ajede, Fan Gu, David Timm, Benjamin Bowers		8. Performing Organization Report No.	
9. Performing Organization Name and Address National Center for Asphalt Technology at Auburn University 277 Technology Parkway Auburn, AL 36830		10. Work Unit No.	
		11. Contract or Grant No. ALDOT Research Project 931-015	
12. Sponsoring Agency Name and Address Alabama Department of Transportation Bureau of Research and Development 1409 Coliseum Boulevard Montgomery, AL 36110		13. Type of Report and Period Covered Final Report June 2020 – November 2022	
		14. Sponsoring Agency Code	
15. Supplementary Notes			
16. Abstract <p>This research project conducted a local verification to assess the accuracy of globally calibrated Pavement ME Design distress and smoothness models for asphalt pavements in Alabama. Pavement sections included LTPP test sections in Alabama and neighboring states, as well as sections tested at the NCAT Test Track.</p> <p>Results showed significant bias in the rutting prediction model for both LTPP and NCAT Test Track sections. The PMED software underpredicted fatigue cracking percentages for general LTPP pavement sections while overpredicting fatigue cracking percentages for NCAT Test Track pavement sections. The IRI prediction model also exhibited significant bias, indicating higher predicted values than measured values.</p> <p>Based on the findings, local calibration of the PMED performance models is essential for accurate predictions under Alabama conditions. Other implementation activities may include validation with independent datasets and training on Pavement ME Design. This project highlights the importance of local verification and calibration to improve prediction accuracy, ensuring more reliable and cost-effective pavement structures.</p>			
17. Key Words Local verification, pavement ME design, rutting, cracking, IRI		18. Distribution Statement No restrictions	
19. Security Classification (of this report) Unclassified	20. Security Classification (of this page) Unclassified	21. No. of Pages 61	22. Price

Acknowledgments

The Alabama Department of Transportation (ALDOT) provided funding for this project. The authors express their gratitude to the ALDOT Project Advisory Committee members, namely Scott George (Chair), Kaye Davis, Virgil Clifton, and Kristy Harris, for their guidance throughout the project and for reviewing the project deliverables.

Table of Contents

Chapter 1 Introduction	8
1.1 Background	8
1.2 MEPDG Design Process	8
1.3 Importance of Local Calibration.....	9
1.4 Objective of the Project	11
1.5 Scope of the Project.....	11
1.6 Organization of the Report	12
Chapter 2 Literature Review	14
2.1 Introduction	14
2.2 Overview of the PMED Software and M-E Design Philosophy	14
2.3 Pavement Performance Prediction Models.....	14
2.3.1 Rutting Prediction Models	15
2.3.2 Load-related Fatigue Cracking Prediction Models.....	16
2.3.3 Transverse/Thermal Cracking Prediction Models.....	17
2.3.4 Smoothness.....	18
2.4 AASHTO Guide for Local Verification and Calibration of PMED	18
2.5 Previous Local Verification and Calibration Efforts by State Highway Agencies	19
2.5.1 Arizona	21
2.5.2 Georgia.....	22
2.5.3 Mississippi	23
2.5.4 Tennessee	23
2.5.5 Louisiana	23
2.5.6 Idaho	24
2.5.7 Summary of Previous Local Calibration Efforts	24
2.6 ALDOT Implementation Status	25
Chapter 3 Methodology	26
3.1 Introduction	26
3.2 Local Verification Procedure	26
3.2.1 Step 1 – Select Hierarchical Input Level for Each PMED Input	26
3.2.2 Step 2 – Select Test Sections.....	27
3.2.3 Step 3 – Extract and Evaluate Distress and Project Data.....	28
3.2.4 Step 4 – Assess Local Bias	28
3.2.5 Step 5 – Assess the Standard Error of the Estimate	28
3.3 Data for LTPP Test Sections	29
3.3.1 LTPP Traffic Inputs	32

3.3.2 Pavement Structure Inputs	34
3.3.3 Climatic Inputs	37
3.4 Data for NCAT Test Track Sections.....	39
3.4.1 Traffic Inputs	40
3.4.2 Pavement Structures and Material Inputs.....	40
3.4.3 Climate Characterization	46
3.4.4 Field Performance Data	46
Chapter 4 Local Verification of PMED Prediction Models	48
4.1 Local Verification.....	48
4.2 Assessment of the Total Rutting Prediction Model	48
4.3 Assessment of the B-U Fatigue and Top-Down Cracking Models	50
4.4 Assessment of the Transverse Cracking Model	52
4.5 Assessment of the IRI Prediction Model	53
Chapter 5 Summary and Conclusions	55
References	56
Appendices.....	58
Appendix A - LTPP Data Extraction Procedure	58
Appendix B - ANNACAP.....	59

List of Tables

Table 1. Local Calibration Efforts by States	21
Table 2. Summary of Local Calibration Efforts Conducted by State Highway Agencies.....	24
Table 3. ALDOT’s Activities for Implementation of Pavement ME Design	25
Table 4. Recommended Hierarchical Input Levels (Darter et al., 2014).....	27
Table 5. Selected LTPP Sections in Alabama for Local Calibration	29
Table 6. Selected LTPP Sections in the Neighboring States.....	31
Table 7. Traffic Input Levels	34
Table 8. Pavement Structure Input Levels	35
Table 9. ANNACAP E* Prediction for LTPP Section 01-4127	37
Table 10. Global Calibration Coefficient of the Distress Prediction Models	48
Table 11. Summary Statistics of the Globally Calibrated Rutting Model	49
Table 12. Summary Statistics of the Globally Calibrated Bottom-Up Fatigue Cracking Model....	50
Table 13. Summary Statistics of the Globally Calibrated Top-Down Cracking Model.....	50
Table 14. Summary Statistics of the Globally Calibrated Transverse Cracking Model	52
Table 15. Summary Statistics of the Globally Calibrated IRI Model	53

List of Figures

Figure 1. Flowchart of Pavement M-E Design Process	9
Figure 2. Improvement of Bias and Precision through Local Calibration (Robbins et al. 2017) ...	10
Figure 3. Bias-Variance Trade-off (Huilgol, 2020)	11
Figure 4. Flowchart of Scope of Work.....	12
Figure 5. Status of Local Calibration of Pavement ME Design for Flexible Pavement	20
Figure 6. LTPP Sections in Alabama and Neighboring States Selected for Local Verification	32
Figure 7. FHWA Vehicle Classification (FHWA, 2013)	33
Figure 8. Hierarchy of Dynamic Modulus Prediction Models (Kim et al., 2011b)	36
Figure 9. Screenshot of Input Data for LTPP Section 01-4127 in ANNACAP.....	36
Figure 10. Weather Stations in Alabama	39
Figure 11. Structural Sections of the 2003 Test Track Cycle (Timm & Priest, 2006)	41
Figure 12. Structural Sections of the 2006 Test Track Cycle (Timm, 2009)	42
Figure 13. Structural Sections of the 2009 Test Track Cycle (Courtesy of David Timm)	43
Figure 14. Structural Sections of the 2012 Test Track Cycle (Courtesy of David Timm)	45
Figure 15. Weather Station at NCAT Test Track	46
Figure 16. ALDOT Beam (Left) and Inertial Profiler (R) (Giler, 2017).....	47
Figure 17. Crack Mapping at the Test Track (Giler, 2017)	47
Figure 18. Comparison of Predicted and Measured Total Rut Depths	49
Figure 19. Comparison of Predicted and Measured Bottom-Up Fatigue Cracking	51
Figure 20. Comparison of Predicted and Measured Top-Down Cracking	52
Figure 21. Comparison of Predicted and Measured Transverse Cracking.....	53
Figure 22. Comparison of Predicted and Measured IRI.....	54

CHAPTER 1 INTRODUCTION

1.1 Background

State highway agencies, such as the Alabama Department of Transportation (ALDOT), have been using the American Association of State Highway and Transportation Officials (AASHTO) 1993 Pavement Design Guide (AASHTO, 1993) and the DARWin program for designing both new pavement and rehabilitation projects. This approach was developed based on the AASHO Road Test conducted between 1958 and 1961 (HRB, 1962). It was later revised as the AASHO Interim Guide for the Design of Pavements, published in 1972 (AASHTO, 1972). The guide was updated as the AASHTO Guide for the Design of Pavements in 1986 (AASHTO, 1986). It was then updated in 1993 (AASHTO, 1993), and it mainly followed the original design methodology, which relies on empirical regression equations that correlate a performance criterion, known as the present serviceability index (PSI), with material properties and traffic loads.

In the early 2000s, the National Cooperative Highway Research Program (NCHRP) introduced a more advanced pavement design methodology called the Mechanistic-Empirical Pavement Design Guide (MEPDG). This approach was developed under NCHRP projects 1-37A and later refined under 1-40D. The MEPDG method uses mechanistic computations to determine pavement responses, such as stresses, strains, and deflections. These responses are then used to predict pavement distress conditions like rutting and cracking, and pavement smoothness, measured by the International Roughness Index (IRI), using performance models. The MEPDG approach has been implemented in the AASHTOWareTM Pavement ME Design (PMED) software for pavement design.

Compared to the AASHTO 1993 Design Guide, MEPDG typically results in thinner asphalt concrete (AC) layers under high traffic (Mashayekhi et al., 2011). This difference can be attributed to the fact that the AASHTO 1993 Design Guide was developed based on the local conditions of the original AASHO Road Test and specific traffic patterns, which have evolved significantly over time. Moreover, the empirical equations in the AASHTO 1993 Design Guide require engineering judgment and extrapolation, especially when designing for traffic loads that exceed those observed in the original AASHO Road Test. Using mechanistic computations in MEPDG eliminates the need for such extrapolation, leading to more rational designs and increasing its consideration for adoption among state highway agencies (SHAs).

1.2 MEPDG Design Process

Figure 1 illustrates the MEPDG design process for flexible pavement as executed in the PMED software. The process begins with the input of design parameters, including a trial pavement structure and data on traffic, climate, and materials. Once executed, the PMED software performs “mechanistic” computations to calculate pavement responses, specifically stresses, strains, and deflections, at critical locations within the pavement structure. Utilizing these computed responses, key pavement performance indicators, namely IRI, rutting, and cracking, are predicted based on “empirical” transfer functions or performance models. The trial pavement

structure is deemed acceptable if its predicted performance meets all predetermined design criteria for its design life. Otherwise, the process is iteratively repeated, either with adjustments to the trial structure or with alternative materials.

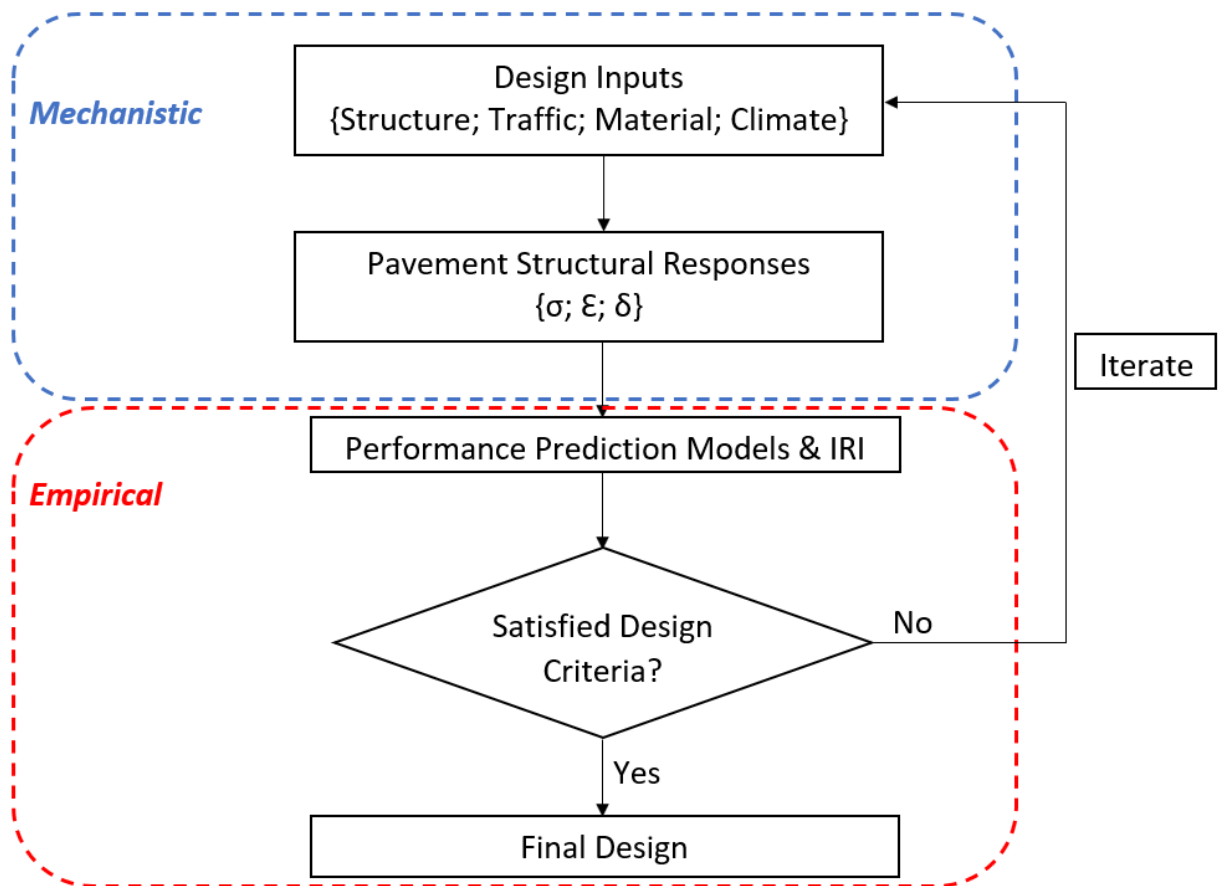


Figure 1. Flowchart of Pavement M-E Design Process

1.3 Importance of Local Calibration

The accuracy of performance predictions made by the PMED software primarily depends on the calibration of the MEPDG transfer models. A comprehensive “global” calibration of these models was conducted by NCHRP (2004) using the Long-Term Pavement Performance (LTPP) database. A set of criteria was considered for selecting suitable pavement sites for this calibration, including:

- Consistent measurements of model inputs and pavement performance
- Sufficient performance observations (at least 3)
- Adequate materials characterization and testing results
- A limited number of pavement layers
- Frequent traffic surveys

Based on these criteria, the study identified 136 LTPP test sections across the United States and Canada, including 94 new sections and 42 overlay sections (NCHRP, 2004). Calibration coefficients were determined to minimize the prediction bias inherent in these transfer models.

While the resulting transfer models represent global conditions, they may not necessarily account for each state's construction and material specifications, pavement preservation and maintenance practices, and traffic and climatic conditions, which are expected to significantly affect pavement performance. Therefore, when implementing the PMED software at a state level, local verification becomes essential to assess if these differences introduce an unacceptable level of bias in performance predictions. If the bias is significant, local calibration becomes necessary to adjust the calibration coefficients of the transfer models. The local calibration process is expected to improve the accuracy of performance predictions.

Figure 2 illustrates how local calibration improves the bias and precision of pavement performance predictions. In practical terms, bias is the difference between the predicted distress at the mean (50%) reliability level and the average measured distress. Precision measures the variance between predicted values at a specified design reliability level and the corresponding measured values.

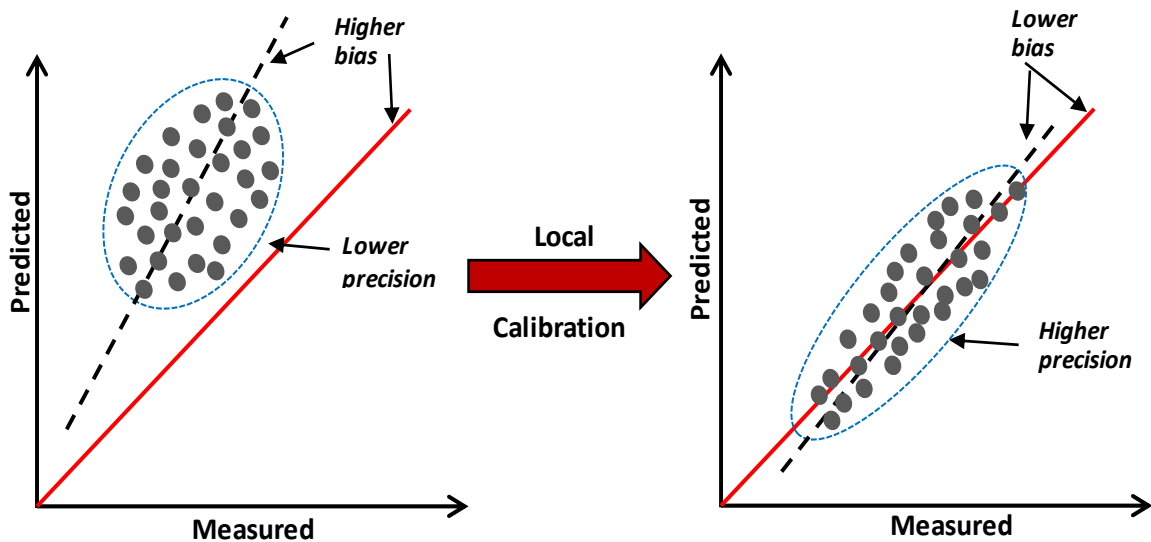


Figure 2. Improvement of Bias and Precision through Local Calibration (Robbins et al. 2017)

The term “local calibration” often includes three steps: local verification, local calibration, and local validation. During local verification for a specific state, performance predictions determined based on globally calibrated transfer functions are compared with distress data measured on the state's flexible pavements. High variance (i.e., low precision) in the comparisons implies that the models capture both the underlying pattern in the data and accompanying noise. In this case, further optimization of the transfer functions is warranted, involving re-calibration (i.e., local calibration) of the models to minimize both bias and variance (i.e., the least total error), as illustrated in Figure 3 and mathematically presented in Equation 1. The irreducible error in Equation 1 measures the noise in the data. Every model has a certain amount of irreducible error or noise that cannot be eliminated.

$$\text{Total Error} = \text{Bias}^2 + \text{Variance} + \text{Irreducible Error} \quad (1)$$

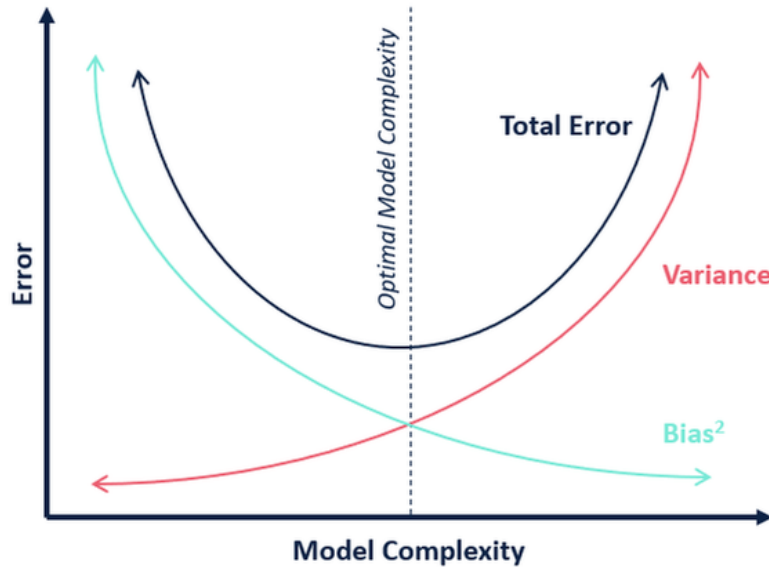


Figure 3. Bias-Variance Trade-off (Huilgol, 2020)

After the local calibration of the performance models, an independent set of data is used to validate the optimized prediction models. The models are considered successfully validated to local conditions if the bias and precision statistics are almost identical to those obtained from a new independent dataset (Tran et al., 2017).

1.4 Objective of the Project

The objective of the project was to examine whether the globally calibrated MEPDG distress and smoothness models could accurately predict distresses and smoothness levels for LTPP flexible pavement test sections in Alabama and neighboring states. The study also evaluated these models against the structural pavement sections tested at the NCAT Test Track. Based on the results of the local verification, a subsequent plan for implementation was developed for consideration by ALDOT.

1.5 Scope of the Project

The project began with a comprehensive literature review to synthesize findings from research efforts conducted by other SHAs in the local verification and calibration of PMED and recent enhancements to the PMED software. Data for LTPP asphalt pavement sections in Alabama and neighboring states were retrieved from the LTPP InfoPave website. The process for extracting and assembling data from the LTPP database involved the following steps:

1. Identifying LTPP flexible pavement test sections in Alabama, as summarized in Appendix A. These include both new and rehabilitated asphalt pavement sections.
2. Identifying LTPP flexible pavement test sections in the neighboring states. These sections were then compared with the LTPP test sections in Alabama to select those with similar pavement structures, materials, and conditions.

3. Extracting and compiling distress/performance data, materials properties, and other relevant information for the selected sections from the LTPP database.

In addition, data from the NCAT Test Track were sourced from the 2003, 2006, 2009, and 2012 research cycles. In each research cycle, the test sections were subjected to approximately two years of heavy truck traffic, equivalent to approximately 10 million Equivalent Single Axle Loads (ESALs) under local climatic conditions. The field performance of the pavement sections on the NCAT Test Track was monitored every week.

Performance predictions of the selected LTPP and Test Track sections were generated using the PMED software (Version 2.6). Local verification involved conducting paired Student t-tests to assess the bias between the measured and predicted distresses and IRI. The results of the local verification process, expressed in terms of bias and standard error, helped determine the need for local calibration of the performance models. Figure 4 illustrates the plan of this study.

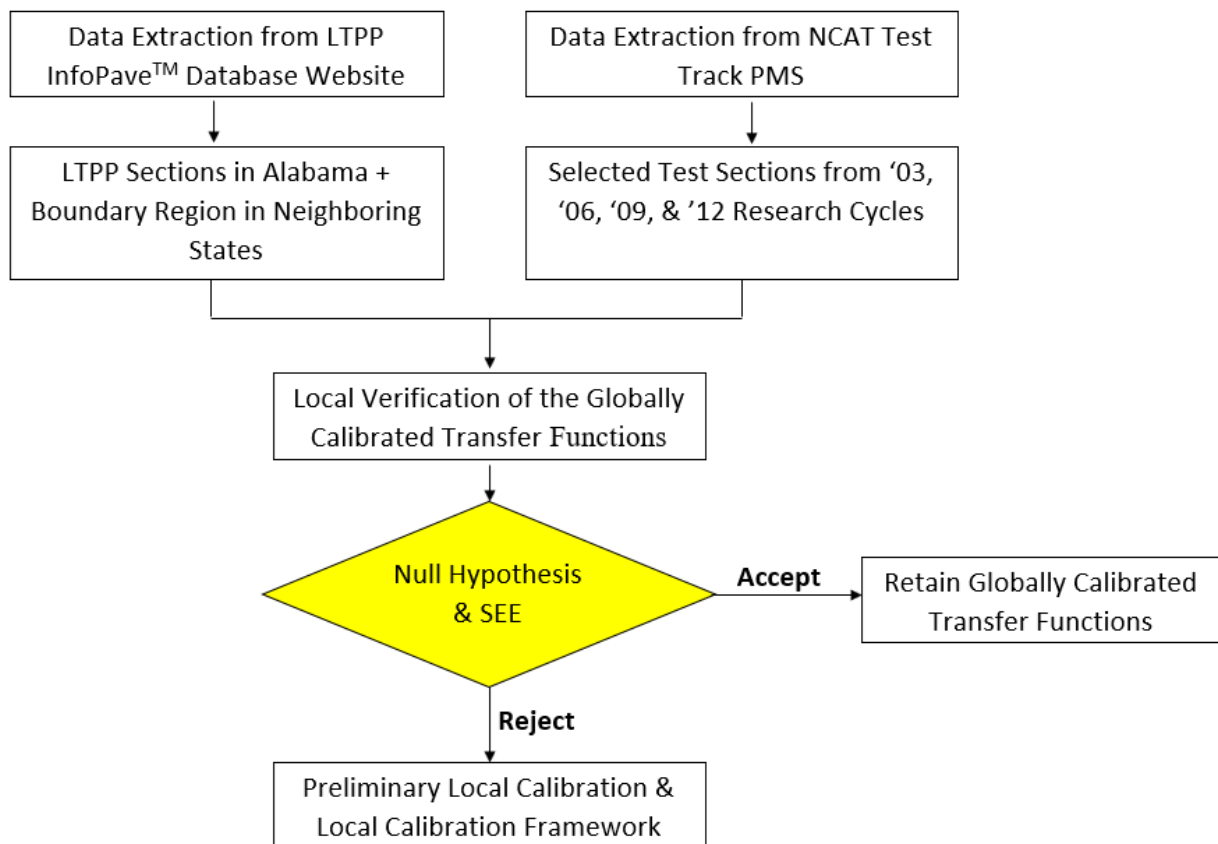


Figure 4. Flowchart of Scope of Work

1.6 Organization of the Report

This report is organized into five chapters. Chapter 1 serves as the introduction, providing background, objectives, scope, and organization of this report. Chapter 2 begins with an overview of the PMED software and MEPDG design philosophy, followed by a literature review of local

calibration efforts conducted by other SHAs. Chapter 3 describes the local verification process. Chapter 4 presents the results of the local verification, using data for the LTPP sections in Alabama and neighboring states and the NCAT Test Track. Finally, Chapter 5 presents the conclusions and recommendations of the study.

CHAPTER 2 LITERATURE REVIEW

2.1 Introduction

Several SHAs have adopted the MEPDG pavement design approach to complement or entirely replace the empirical AASHTO 1993 Pavement Design Guide. However, before integrating MEPDG into routine pavement design practices, it is crucial to verify the globally calibrated transfer models in PMED through local verification and calibration. This review summarizes the previous works by SHAs and other stakeholders in the local verification and calibration efforts.

Insights from prior efforts indicate that local calibration of models for smoothness (i.e., IRI) and transverse cracking was relatively straightforward. However, the local calibration of the fatigue cracking model has been challenging. This difficulty was attributed to the poor fit of the globally calibrated fatigue cracking model (Von Quintus et al., 2007).

This chapter provides an overview of the PMED software and its key performance indicators, followed by a discussion of the AASHTO Guide for local verification and calibration of PMED. Finally, the chapter concludes with a summary of previous efforts in local verification and calibration by SHAs.

2.2 Overview of the PMED Software and M-E Design Philosophy

The PMED software has seen multiple updates through research projects sponsored by NCHRP and the Federal Highway Administration (FHWA). Additionally, evaluations from SHAs and other key stakeholders in the industry have contributed to its refinement (AASHTO, 2020). For this study, the PMED software Version 2.6 was employed.

The MEPDG Manual of Practice (AASHTO, 2020) outlines a three-step process for using the PMED software in the design of new constructions, overlays, and restorations:

1. Create a trial design.
2. Execute the PMED software for the trial design to predict key distresses and IRI.
3. Review the predicted performance based on selected performance criteria and reliability levels, then adjust the trial design as needed.

The PMED software computes cumulative pavement distresses by integrating mechanistic pavement responses (i.e., stress, strain, and deflection) with empirical transfer functions. PMED can predict a range of pavement performance indicators, including smoothness, permanent deformation (i.e., rutting) in individual layers, overall rutting, bottom-up and top-down fatigue cracking, reflective cracking, and transverse (i.e., thermal) cracking (Bayomy et al., 2018).

2.3 Pavement Performance Prediction Models

The PMED software features performance (i.e., distress) prediction models globally calibrated using an extensive dataset from roadway sections across North America. Primary data sources include the LTPP database. Additional data were gathered from the MnRoad experiment and various state DOT research initiatives (AASHTO, 2020). Given the diverse range of pavement features represented in the global calibration, local calibration by state-level DOTs is crucial for generating performance predictions that closely align with local field conditions. The following sections provide details for MEPDG performance prediction models, including the International

Roughness Index (IRI), rutting, load-related cracking (namely, fatigue cracking), and non-load-related cracking (such as transverse cracking).

2.3.1 Rutting Prediction Models

Rutting is a form of pavement distress due to the permanent deformation in each pavement layer, resulting in surface depression along the wheel path. The rut depth in a pavement is the maximum vertical elevation difference between the transverse profile of the AC surface and a line across the lane width. The PMED software calculates rut depth within the AC, unbound aggregate layers, and the subgrade in inches. Rutting prediction is computed using two different rutting models. The first model, as defined in Equation 2, predicts rutting in the AC layer, while the second model, represented as Equation 3, predicts rutting in the unbound base and subgrade layers of the pavement (AASHTO, 2020).

$$\Delta_{p(AC)} = \varepsilon_{p(AC)} h_{AC} = \beta_{1r} K_z \varepsilon_{r(AC)} 10^{k_{1r} n^{k_{3r} \beta_{3r}} T^{k_{2r} \beta_{2r}}} \quad (2)$$

Where:

$\Delta_{p(AC)}$	= Accumulated permanent or plastic vertical deformation in the AC layer/sublayer, in.
$\varepsilon_{p(AC)}$	= Accumulated permanent or plastic axial strain in the AC layer/sublayer, in/in.
$\varepsilon_{r(AC)}$	= Resilient or elastic strain calculated by the structural response model at the mid-depth of each AC sublayer, in/in.
h_{AC}	= Thickness of the AC layer/sublayer, in.
n	= Number of axle load applications
T	= Mix or pavement temperature, °F
$k_{1r, 2r, 3r}$	= Global lab-derived coefficients for dense-graded neat AC mixture ($k_{1r} = 2.4545, k_{2r} = 3.01, k_{3r} = 0.22$)
$\beta_{1r}, \beta_{2r}, \beta_{3r}$	= Local or mixture calibration or field-shift constants; for global calibration, these constants are: $\beta_{1r} = 0.40, \beta_{2r} = 0.52$, and $\beta_{3r} = 1.36$
K_z	= Depth confinement factor

$$\delta_i = \beta_1 K_1 \left(\frac{\varepsilon_0}{\varepsilon_r} \right) e^{-(\rho/N)^\beta} \varepsilon_v h_i \quad (3)$$

Where:

δ_i	= Rut deformation in the sublayer i , in.
β_1	= Local calibration coefficient of unbound materials, where β_b represents granular base and β_s is for subgrade layer.
K_1	= Regression model coefficient (i.e., default value of 2.03 for base and 1.35 for subgrade)
$\varepsilon_0/\varepsilon_r$	= Obtained in the lab or estimated based on material field investigation.

β, ρ	= Unbound material properties.
N	= Number of axle load applications.
ε_v	= Vertical resilient strain of the sublayer i under load application
h_i	= Thickness of the sublayer i , in.

2.3.2 Load-related Fatigue Cracking Prediction Models

Load-related fatigue cracking in asphalt pavements includes two types: bottom-up fatigue cracking, commonly known as alligator cracking, and top-down fatigue cracking. Bottom-up fatigue cracking can be found in thin asphalt pavements. It initiates at the bottom of the asphalt layer where tensile stress is the highest. It propagates upward to the asphalt surface due to the stress caused by repeated traffic loads.

Conversely, top-down fatigue cracking is usually observed in thick pavements, where cracks are more likely to initiate at the top of the surface layer. This is due to the concentration of tensile stresses resulting from tire-pavement interaction and the aging of the asphalt binder. These cracks extend downward through the layer under the ongoing traffic.

The prediction models for bottom-up fatigue cracking (expressed as a percentage of the total lane area) and the length of top-down fatigue cracks (i.e., longitudinal cracking) are presented in Equations 4 and 12, respectively.

$$FC_{Bottom-up} = \left(\frac{6000}{1 + e^{(C_1 \times C_1^* + C_2 \times C_2^* \log(100 \times DI_{bottom-up}))}} \right) \quad (4)$$

Where:

$FC_{Bottom-up}$ = bottom-up fatigue cracking.
 C_1^* and C_2^* = coefficients that can be computed using Equations 5 and 6.

$$C_1^* = -2 \times C_2^* \quad (5)$$

$$C_2^* = -2.40874 - 39.748(1 + h_{HMA})^{-2.856} \quad (6)$$

Where:

h_{HMA} = total HMA thickness.
 $DI_{Bottom-up}$ = damage index that is calculated using Equation 7.

$$DI_{Bottom-up} = \sum (\Delta DI)_{j,m,l,p,T} = \sum \left(\frac{N}{N_{f-HMA}} \right)_{j,m,l,p,T} \quad (7)$$

$$N_{f-HMA} = k_{f1}(C)(C_h)\beta_{f1}(\varepsilon_t)^{k_{f2}}\beta_{f2}(E)^{k_{f3}}\beta_{f3} \quad (8)$$

Where:

ΔDI = incremental damage index.
 N = actual number of axle load applications within a specific period.
 j = axle load interval.

m	= axle load type (single, tandem, tridem, quad, or special axle configuration).
l	= truck type using the truck classification groups included in the MEPDG.
p	= month.
T	= median temperature for the five temperature intervals used to subdivide each month.
N_{f-HMA}	= allowable number of axle load applications for a flexible pavement to fatigue cracking.
ε_t	= tensile strain at the critical location.
E	= dynamic modulus measured in compression.
k_{f1}, k_{f2}, k_{f3}	= global field calibration parameters (from NCHRP 1-40D recalibration (Darter et al., 2006), $k_{f1} = 0.007566$, $k_{f2} = -3.9492$, $k_{f3} = -1.281$).
$\beta_{f1}, \beta_{f2}, \beta_{f3}$	= local or mixture field calibration factors; these factors were all set to 1.0 for the global calibration.
C	= constant depending on mix properties (Equations 9 and 10):

$$C = 10^M \quad (9)$$

$$M = 4.84 \left(\frac{V_{be}}{V_a + V_{be}} - 0.69 \right) \quad (10)$$

Where:

V_a	= air voids (in %) at the time the roadway was opened to traffic.
V_{be}	= effective asphalt content by volume of the mix (in %) placed on the roadway.
C_h	= thickness correction in term (Equation 11):

$$C_h = \frac{1}{0.000398 + \frac{0.003602}{1 + e^{(11.02 - 3.49 \times h_{HMA})}}} \quad (11)$$

$$FC_{Top-Down} = 10.56 \left(\frac{C_4}{1 + e^{[(C_1 - C_2) \log(DI_{Top})]}} \right) \quad (12)$$

Where:

$FC_{Top-Down}$	= Length of top-down (longitudinal) cracking, ft/mi.
DI_{Top}	= Cumulative damage index near the top of the AC surface.
$C_{1,2,4}$	= Regression constants, $C_1 = 7.0$, $C_2 = 3.5$, and $C_4 = 1000$.

2.3.3 Transverse/Thermal Cracking Prediction Models

Transverse thermal cracking is a non-load related pavement distress usually caused by asphalt pavement surface shrinkage in response to low temperatures or asphalt binder hardening. These cracks are perpendicular to the pavement's centerline or the direction of travel (Pavement Interactive, 2021). Equation 13 shows the prediction model for this form of cracking.

$$TC = \beta_{t1} N \left[\frac{1}{\sigma_d} \left(\frac{C_d}{h_{HMA}} \right) \right] \quad (13)$$

Where:

TC	= amount of thermal cracking, ft/mi.
β_{t1}	= regression coefficient determined through global calibration, $\beta_{t1} = 400$.
N	= standard normal distribution.
σ_d	= standard deviation of the log of the depth of cracks in the pavement, $\sigma_d = 0.0769$ in.
C_d	= crack depth, in.
h_{HMA}	= thickness of HMA layers.

2.3.4 Smoothness

The International Roughness Index serves as a key metric for assessing pavement smoothness. In the MEPDG framework, IRI is empirically predicted over a design period as a function of pavement distresses, site-specific conditions, and the initial IRI value, as shown in Equation 14 (AASHTO, 2020).

$$IRI = IRI_0 + C_1 \times RD + C_2 \times FC_{total} + C_3 \times TC + C_4 \times SF \quad (14)$$

Where:

IRI_0	= Initial IRI value before traffic loading
C_1, C_2, C_3, C_4	= Local calibration coefficients (national values or defaults: $C_1 = 40$, $C_2 = 0.4$, $C_3 = 0.008$, $C_4 = 0.015$)
RD	= Average rut depth, in.
FC_{total}	= Total area of load-related cracking (i.e., fatigue cracking, longitudinal, and reflection cracking), percent
TC	= Total length of transverse cracks, ft/mile
SF	= Site factor

$$SF = Age[0.02003 * (PI + 1) + 0.007947 * (Precip + 1) + 0.000636 * (FI + 1)] \quad (15)$$

Where:

Age	= Pavement age in years
PI	= Percent of plasticity index of the soil
FI	= Annual freezing average index, °F days
$Precip$	= Average annual precipitation or rainfall, in.

2.4 AASHTO Guide for Local Verification and Calibration of PMED

The AASHTO Guide for Local Verification and Calibration of the PMED (AASHTO, 2010) describes a detailed step-by-step procedure for local calibration. This procedure involves several key steps:

1. Collecting input parameters.
2. Estimating sample size for assessing transfer models.

3. Selecting representative roadway segments.
4. Conducting field and forensic investigations of test sections.
5. Assessing local bias and standard error of the estimate.
6. Minimizing local bias and standard error of the estimate.
7. Validating the calibrated transfer models using an independent dataset.

To ensure accurate calibration, the local calibration procedure recommends a minimum number of pavement segments for each transfer model. Specifically, for rutting, a minimum of 20 segments is recommended. For load-related cracking (e.g., bottom-up and top-down cracking), it is recommended to have 30 segments. In the case of non-load related cracking (e.g., thermal cracking), 26 segments are recommended. Ideally, the selected segments should have at least three condition surveys conducted in the past 10 years.

In this procedure, Steps 5 through 7 are referred to as local verification, calibration, and validation, respectively. During the local verification process (Step 5), the PMED software with global calibration factors is utilized to design pavements with inputs gathered from the selected pavement segments at a 50% reliability level. For each performance model, predicted distresses are plotted and compared with the measured distresses for which linear regression is performed.

2.5 Previous Local Verification and Calibration Efforts by State Highway Agencies

Several states have already calibrated, or are in the process of calibrating, the pavement performance models within the PMED software to better align them with local conditions. Figure 5 shows the most recent status of PMED local calibration efforts for flexible pavements across the country, indicating that 28 states have already completed local calibration, while 8 states are currently conducting calibration efforts. Table 1 summarizes their verification and calibration efforts for each performance model. The following sections provide an overview of the major findings and observations of these efforts.

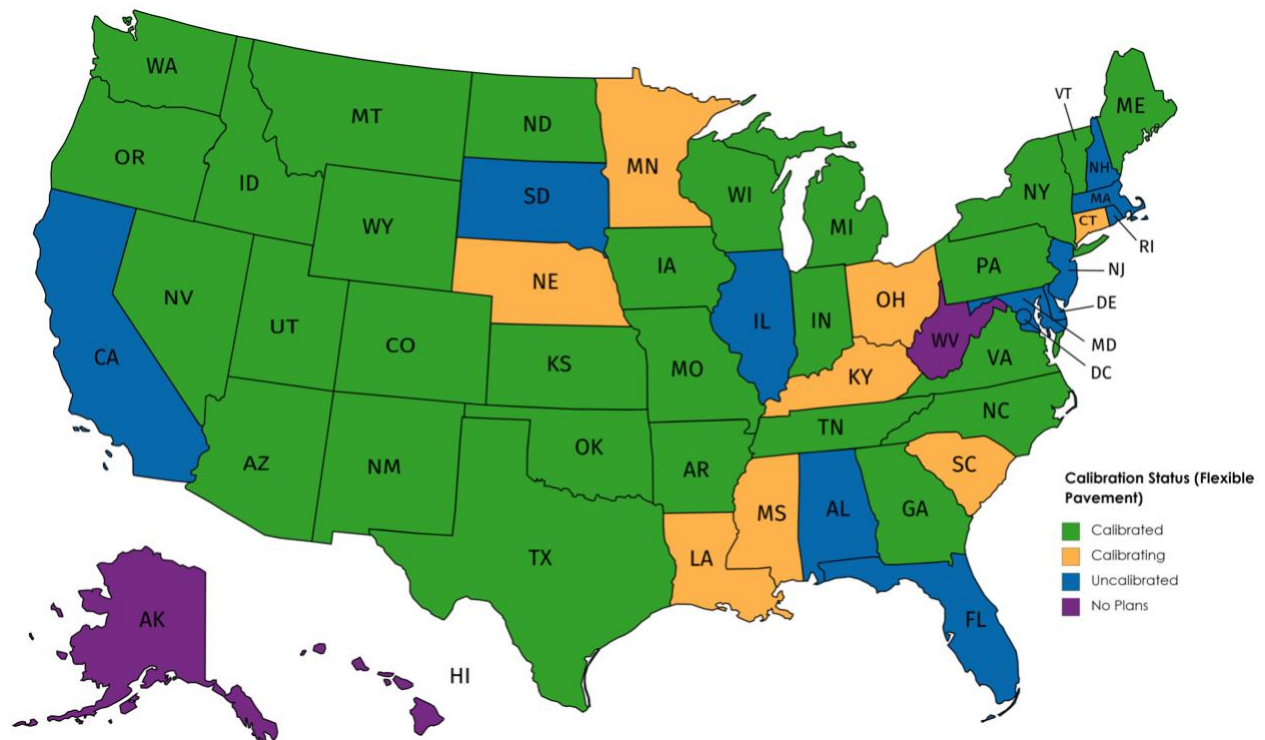


Figure 5. Status of Local Calibration of Pavement ME Design for Flexible Pavement

Table 1. Local Calibration Efforts by States

State/ Region	Sponsoring Agency	Year of Publication	Verification (V)/Calibration (C)									
			Fatigue Cracking		Rutting		Transverse Cracking		IRI		Long. Cracking	
			V	C	V	C	V	C	V	C	V	C
AZ	AZ DOT	2014	✓	✓	✓	✓	✓	✓	✓	✓		
CO	CO DOT	2013	✓	✓	✓	✓	✓	✓	✓	✓		
GA	GDOT	2016	✓	✓	✓	✓	✓	✓	✓	✓		
IA	IA DOT	2013	✓		✓	✓	✓		✓	✓	✓	✓
ID	ID DOT	2018	✓	✓	✓	✓	✓	✓	✓	✓	✓	✓
KS	KS DOT	2015	✓		✓	✓	✓	✓	✓	✓	✓	✓
LA	LA DOTD	2012	✓		✓				✓			
MI	MI DOT	2014	✓	✓	✓	✓	✓	✓	✓	✓	✓	✓
MN	MN DOT	2009	✓	✓	✓		✓	✓			✓	
MO	MO DOT	2007	✓		✓	✓	✓	✓	✓		✓	
MS	MS DOT	2017	✓	✓	✓	✓	✓	✓	✓	✓		
NC	NC DOT	2011	✓	✓	✓	✓						
NM	NM DOT	2013	✓	✓	✓	✓			✓	✓	✓	✓
Northeast	NYS DOT	2011	✓	✓	✓	✓	✓		✓	✓		
OH	OH DOT	2009			✓	✓	✓		✓	✓		
OR	OR DOT	2013	✓	✓	✓	✓	✓	✓			✓	✓
NV	UNR	2015	✓	✓	✓	✓						
TN	TN DOT	2013			✓				✓			
TX	TX DOT	2014	✓	✓	✓	✓	✓	✓				
UT	UT DOT	2009	✓		✓	✓	✓		✓			
VA	VDOT	2015	✓	✓	✓	✓			✓	✓		
WA	WS DOT		✓	✓	✓	✓	✓		✓		✓	✓
WI	WI DOT	2012	✓	✓	✓	✓						
WY	WY DOT	2015	✓	✓	✓	✓	✓	✓	✓			

2.5.1 Arizona

Darter et al. (2014) conducted verification, calibration, and validation of fatigue cracking, transverse cracking, rutting, and IRI models in the PMED software. They utilized field performance data from flexible pavement sections in Arizona for the study. During verification, they compared the distress predictions made by PMED, which used default global calibration coefficients, with the measured pavement performance data. The comparison showed a significant bias in the predicted pavement performance, necessitating calibration to local conditions. To validate the calibrated models, the researchers withheld 10% of the Arizona performance data and conducted a sensitivity analysis.

Additionally, the study observed transverse cracking at intervals of approximately 50 to 200 feet in both LTPP and Pavement Management System (PMS) sections. These sections were located in traditionally non-frost regions of Arizona, which contradicts the expected pavement failure mechanisms in such climates. Standard transverse cracking models generally assume that low-temperature contraction of asphalt binders generates tensile stresses, leading to transverse cracks in the pavement. However, these cracks were observed in warmer areas of Arizona, leading the researchers to speculate that they may have originated from significant shrinkage in the Hot-Mix Asphalt (HMA) mixture, possibly due to the aggregates absorbing the binder. This finding led the researchers to suggest the need for further study to create a thermal cracking prediction model that accounts for warm, non-frost regions of the state.

2.5.2 Georgia

The Georgia Department of Transportation (GDOT) currently uses the 1972 AASHTO interim guide for designing flexible pavements but is considering transitioning to PMED for new and rehabilitated flexible pavements. To assist GDOT in this transition, Von Quintus et al. (2014) conducted local verification and calibration of the transfer functions in PMED, using data from 38 flexible pavement sections in Georgia, including 22 LTPP test sections and 16 non-LTPP roadway sections. The research involved comparing predicted performance values from PMED to field-measured values.

Their findings showed low bias in the fatigue cracking model. However, the models for rutting, thermal cracking (or transverse cracking), and IRI exhibited significant bias with poor goodness-of-fit. To reduce prediction bias, they conducted local calibration and proposed a series of calibration coefficients for Georgia conditions. They also reported that using back-calculated elastic layer modulus values resulted in significantly less prediction bias for rut depth compared to using laboratory-measured resilient modulus values.

The implementation of PMED in Georgia comprised three phases, including (1) verification of PMED transfer functions and associated global calibration coefficients, (2) evaluation of the applicability of these global calibration coefficients by comparing predicted and measured distress data for Georgia LTPP and non-LTPP sections, and (3) calibration of transfer functions that exhibited significant prediction bias. Notably, longitudinal cracking was not considered in the local calibration, as the MEPDG Manual of Practice discouraged the inclusion of longitudinal transfer functions in design decisions. The study included 18 test sections, as recommended in the AASHTO MEPDG Local Calibration Guide (Von Quintus et al., 2016).

Lastly, Von Quintus et al. (2016) noted considerable variance between measured and predicted transverse cracks. Like observations made by Darter et al. (2014), they suggested that the mechanism behind the measured transverse cracks in selected Georgia sections likely involved a combination of low-temperature contraction and shrinkage. They also emphasized that this shrinkage mechanism has yet to be incorporated into the PMED software.

2.5.3 Mississippi

Von Quintus et al. (2017) conducted local verification and preliminary local calibration of the PMED software for the Mississippi Department of Transportation (MDOT). They used both LTPP and non-LTPP sections in Mississippi for the local calibration of pavement transfer functions that exhibited significant bias and poor precision. The verification and calibration process covered various types of flexible pavement structures, including thick and thin conventional flexible pavements (comprising asphalt concrete over an aggregate base with or without a stabilized subgrade layer), full-depth flexible pavements (including asphalt concrete placed directly on embankment soil or lime-stabilized soil), semi-rigid pavements (featuring asphalt concrete over cement or lime-treated base), and asphalt overlays of these flexible pavements. Data encompassing traffic, climate, structural details, and material properties were sourced from 36 LTPP test sections and 70 non-LTPP roadway segments.

The local verification results indicated moderate prediction bias in the fatigue cracking and IRI models for flexible pavements in Mississippi. However, the models for rutting and transverse cracking still showed significant bias. As previously reported in local calibration efforts in Georgia (Quintus et al., 2016) and Arizona (Darter et al., 2014), the transverse cracking transfer function yielded predictions that deviated significantly from the measured values. This discrepancy was attributed to a combination of low-temperature and shrinkage mechanisms in the flexible pavement. Consequently, the researchers suggested an iterative approach that maximized goodness-of-fit by fine-tuning the coefficients in each transfer function. They also recommended additional field investigations, particularly of non-LTPP sections, to further minimize the standard error of the transfer functions.

2.5.4 Tennessee

Zhou et al. (2013) and Gong et al. (2017) utilized data from the Highway Pavement Management Application of Tennessee to perform local calibration of PMED. Their research showed that PMED tended to under-predict bottom-up alligator cracking while over-predicting rut depth, top-down longitudinal cracking, and IRI of asphalt pavements in Tennessee. To mitigate prediction bias, they determined local calibration coefficients and validated the calibrated models using the Jackknife method. However, due to the lack of performance data, they did not conduct verification or calibration of the transverse cracking model.

2.5.5 Louisiana

Wu and Yang (2012) conducted a verification study on PMED in Louisiana. They evaluated the precision and bias of fatigue cracking, rutting, and IRI transfer functions using data from 40 flexible pavement sections. These sections encompassed five typical pavement structures: AC over AC base, AC over rubblized Portland cement concrete (RPCC) base, AC over crushed stone, AC over soil cement base, and AC over stone interlayer pavements. The data was extracted from the Louisiana Department of Transportation and Development's (LADOTD) network-level pavement management system (LA-PMS) and other state project-tracking databases.

The study found that the globally calibrated models for load-related fatigue cracking, rutting, and IRI were adequate for predicting distress in AC over AC base pavements in Louisiana. The transfer functions were also satisfactory for the AC over RPCC, except for the rutting model, which would require local calibration. However, for AC over soil cement base pavements in Louisiana, the predicted fatigue cracking was significantly less than the measured field performance. Conversely, rutting was over-predicted, as compared to the field performance data. Only the IRI regression model was found to be adequate. The study concluded that local calibration would be needed, particularly for AC over soil cement base pavements.

2.5.6 Idaho

Bayomy et al. (2018) conducted a local calibration study across 32 pavement sites in Idaho, considering a range of geographical, climatic, and traffic conditions. Data were collected from the Idaho Transportation Asset Management System. Their findings indicated that PMED tended to overestimate rut depth and top-down longitudinal cracking but underestimated bottom-up alligator cracking and transverse cracking. To address these discrepancies, they employed a split-sample approach, dividing the sites into a calibration dataset (26 sites) and a validation dataset (six sites). The subsequent calibration significantly improved the prediction accuracy, and the calibrated models demonstrated a satisfactory goodness-of-fit for the six validation sites.

2.5.7 Summary of Previous Local Calibration Efforts

Table 2 summarizes the local calibration efforts by the state highway agencies discussed in this section.

Table 2. Summary of Local Calibration Efforts Conducted by State Highway Agencies

Study	Scope	Major Outcomes
Darter et al. (2014)	Local calibration of PMED performance models for Arizona.	The globally calibrated distress and smoothness models of asphalt and rigid pavements were locally verified, calibrated, and validated.
Von Quintus et al. (2014)	Local calibration of PMED performance models for Georgia.	Transfer functions showed a significant bias between the measured and predicted pavement distress, prompting a need for local calibration.
Von Quintus et al. (2017)	Local calibration of PMED performance models for Mississippi.	Local calibration of the PMED performance models is pending the completion of field investigations for the non-LTPP test sites.
Zhou et al. (2013)	Local verification of PMED performance models for Tennessee.	The globally calibrated rutting model was adequate with Level 1 data input but overpredicted rutting with Level 3 data input. Traffic levels significantly influenced (IRI).
Wu & Yang (2012)	Local verification of PMED performance models for Louisiana.	Globally calibrated models generally overpredicted rutting distress, except for AC over AC base pavements, and yielded adequate predictions for fatigue cracking, except in AC over soil cement base pavements.
Bayomy et al. (2018)	Local calibration of PMED performance models for Idaho.	The globally calibrated models overpredicted rutting and underpredicted transverse cracking, while adequately predicting bottom-up fatigue cracking.

2.6 ALDOT Implementation Status

ALDOT has sponsored several research initiatives aimed at implementing PMED. Table 3 provides a summary of implementation activities supported by ALDOT. Timm et al. (2010) identified five essential areas for effective implementation. These include PMED training, conducting comparative designs using existing and new methodologies, developing a material reference library specific to PMED, generating monthly distributions, vehicle classes, and axle load distributions, and executing local verification and calibration. In collaboration with Auburn University, ALDOT has developed a brief training course titled "Introduction to M-E Design Short Course." This course comprises modules that align with the PMED workflow, covering general design properties, traffic, climate, materials, and performance prediction interpretation (Timm and Turochy, 2011). Turochy et al. (2005) formulated traffic factors and axle load distribution models for ALDOT, utilizing WIM data from 13 sites. They also conducted a sensitivity analysis to assess the influence of truck factors on the design thickness of flexible pavement. Additionally, ALDOT is currently sponsoring a study to develop a material reference library for PMED.

Table 3. ALDOT's Activities for Implementation of Pavement ME Design

Critical Area for Implementation	ALDOT's Activities
Traffic	Developed traffic factor and axle load spectra
Material Reference Library	Ongoing research study
Local Verification and Calibration	Funded through this project
Training	Introduction to M-E Design Short Course
Concurrent Design	Not available

CHAPTER 3 METHODOLOGY

3.1 Introduction

The success of this study depends on both the quality of the data and the methodology used for local verification of globally calibrated transfer functions. To achieve the study's objectives, data were sourced from (1) the LTPP database for all asphalt pavement test sections in Alabama and selected asphalt pavement test sections in neighboring states, and (2) the NCAT Test Track database. The selected LTPP asphalt pavement test sections from neighboring states were those located near the Alabama state lines.

This chapter begins by outlining the procedure followed in this study for local verification, which closely aligns with the standard local calibration protocol described in the AASHTO guidelines (AASHTO, 2010). It is followed by a discussion on the methodology for extracting LTPP data and the computation of additional inputs necessary for conducting pavement design using the PMED software, as part of the local verification process.

3.2 Local Verification Procedure

Local verification can considerably enhance the efficacy of the PMED procedure by ensuring the adequacy of globally calibrated transfer functions. This section outlines the step-by-step approach for local verification, focusing on transfer functions correlating pavement responses to performance characteristics.

3.2.1 Step 1 – Select Hierarchical Input Level for Each PMED Input

The first step in local calibration involves hierarchical input selection, aimed at characterizing as-constructed pavements in the PMED software for performance prediction and comparison with measured values. As performance prediction directly relies on the chosen input parameters, PMED offers three levels of inputs to enhance prediction accuracy based on available data. Each design input level, ranging from site-specific measurements to user-selected average values, is defined in the MEPDG Manual of Practice (AASHTO, 2020).

- Level 1: This highest level consists of site-specific, high-quality inputs. These inputs are directly measured either in the lab or in the field. For example, Level 1 traffic data includes on-site measurements of axle load distribution and truck classification.
- Level 2: These inputs are derived from regression equations or correlated data, offering a cost-effective alternative to direct measurements. They represent regional-level data.
- Level 3: These are user-selected average values for a specific region and are less reliable.

The choice of input level is influenced by the agency's lab capabilities, material, and construction specifications (AASHTO, 2010). The input level recommended for each PMED input by Darter et al. (2014) is presented in Table 4.

Table 4. Recommended Hierarchical Input Levels (Darter et al., 2014)

MEPDG Input Variable	Sensitivity to Predicted Distress/ Smoothness				Input Level
	Alligator Cracking	Rutting	Transverse Cracking	IRI	
HMA thickness	xxx	xx	x	xx	Level 1
HMA coefficient of thermal contraction			xx		Levels 2 and 3
HMA dynamic modulus	xx	xxx			Level 2
HMA air voids in situ (at placement)	xxx	xxx	xx		Level 3
Effective HMA binder content	xxx	xx	xx	x	Level 3
HMA creep compliance	xx	xxx	xxx		Level 1
HMA tensile strength			xxx		Level 3
Base type/modulus	xxx	xx			Level 2
Base thickness	x				Level 1
Subgrade type/modulus	xx	xx			Level 1
Groundwater table	x	x			Level 3
Climate	xx	xx	xxx	x	Level 2
Truck volume	xxx	xxx			Level 2
Truck axle load distribution	x	x			Level 2
Tire load, contact area, and pressures	xx	xxx			Level 3
Truck speed	xx	xxx			Level 3
Truck wander	xx	xx			Level 3
Initial IRI				xxx	Level 2

* x, xx, and xxx represent the small, medium, and large effects on distress/IRI, respectively.

3.2.2 Step 2 – Select Test Sections

Three types of experimental test sections have been used for developing and calibrating the performance models in the PMED software:

- Long-term full-scale sections, which encompass PMS and research-grade segments such as LTPP test sections.
- Accelerated Pavement Testing (APT) pads with simulated truck loadings.
- APT with full-scale truck loadings, commonly known as test tracks.

Long-term full-scale sections, specifically LTPP test sites, are well-suited for local verification of the globally calibrated performance models in the PMED software. APT pads with simulated truck loadings are useful for verifying transfer functions, assessing specific factors influencing pavement distress, evaluating bias, and measuring variance in transfer functions. Test tracks are effective for local calibration of the globally calibrated transfer functions. Due to controlled variables, lower standard errors in estimates are expected for these test track sections.

This study includes selected sections from the NCAT test track and LTPP test sites for local verification. Following the guidelines (AASHTO, 2010), chosen sections have consistent time intervals between measurements and offer at least three condition surveys.

3.2.3 Step 3 – Extract and Evaluate Distress and Project Data

This step involves data collection and identifying missing elements essential for PMED analysis. It comprises three sub-steps:

1. Extract, review, and convert the measured distress data into a format consistent with PMED predictions.
2. Compare the maximum measured distress data to the threshold values or design criteria of the state agency.
3. Evaluate the measured distress data of all test sections for outliers and anomalies.

3.2.4 Step 4 – Assess Local Bias

This step is to identify any potential bias in the globally calibrated transfer functions. The PMED is used to predict the performance of each test section using the average input values at a 50% reliability. The PMED predictions are then used to assess local bias in two sub-steps:

1. Calculate Residual Errors and Bias: Compute the residual errors, bias, and Standard Error of the Estimate (S_e) for each transfer function. Prepare a plot with a reference line of equality to provide an overview of any existing bias and variance between the measured and predicted distresses.
2. Conduct Hypothesis Testing: To confirm the existence of bias between measured and predicted distresses, a hypothesis test is applied to the data pool. The default null hypothesis asserts no bias or difference between the measured and predicted distresses, as shown in Equation 16. In this study, a paired Student's t-test is utilized for the hypothesis testing.

$$H_0: \sum(y_{measured} - x_{predicted}) = 0 \quad (16)$$

where:

$$\begin{aligned} y_{measured} &= \text{measured value} \\ x_{predicted} &= \text{predicted value by PMED software} \end{aligned}$$

3.2.5 Step 5 – Assess the Standard Error of the Estimate

This step in the local verification process focuses on comparing the standard error derived from both measured and predicted data to the standard error calculated from the global dataset. Robbins et al. (2017) recommend local calibration if the locally verified standard error exceeds the global standard error. The decision for local calibration ultimately depends on the criteria set by the state agency. The Standard Error can be adjusted by modifying the calibration coefficients, as suggested in the NCHRP 1-40 report (AASHTO, 2020).

3.3 Data for LTPP Test Sections

The data essential for the local verification of pavements in Alabama was sourced from two databases: the LTPP InfoPave™ and the NCAT Test Track. Extracting data from the InfoPave™ website requires a combination of appropriate filters. In this study, data from the LTPP test sections in Alabama and the selected LTPP test sections in neighboring states were extracted by applying the following two filters:

- Filter by Surface Type
- Filter by Experiment Type

The selected Surface Type in the data extraction process was asphalt concrete pavement (ACP). Experiment Type filters were then applied to restrict data extraction to asphalt pavement structures suitable for local verification. A total of 52 out of 68 available asphalt pavement test sections in Alabama met these criteria, and they are from the following LTPP experiments:

- General Pavement Studies (GPS)-1 – Asphalt Concrete (AC) on Unbound Granular Base (UB)
- GPS-2 – AC on Bound Base (BB)
- GPS-6 – AC Overlay of AC Pavement
- Specific Pavement Studies (SPS)-1 – Structural Factors for Flexible Pavements
- SPS-3 – Preventive Maintenance of AC Pavement
- SPS-5 – AC Overlay of AC Pavement

Table 5 presents general information about the 51 selected LTPP sections in Alabama. It is important to note that one LTPP section (01-A310) out of the 52 selected sections was excluded due to a lack of critical input data. The selected LTPP sections from neighboring states are presented in Table 6. The LTPP data extraction process is summarized in Appendix A.

Table 5. Selected LTPP Sections in Alabama for Local Calibration

SHRP_ID	Experiment	Pav. Structure*	Functional Class	Route	Const. Year	AADTT
01-0101	SPS-1	AC over UB	Rural Principal Arterial	US 280 West	1993	730
01-0102	SPS-1	AC over UB	Rural Principal Arterial	US 280 West	1993	730
01-0103	SPS-1	AC over BB	Rural Principal Arterial	US 280 West	1993	730
01-0104	SPS-1	AC over BB	Rural Principal Arterial	US 280 West	1993	730
01-0105	SPS-1	AC over BB	Rural Principal Arterial	US 280 West	1993	730
01-0106	SPS-1	AC over BB	Rural Principal Arterial	US 280 West	1993	730
01-0107	SPS-1	AC over BB	Rural Principal Arterial	US 280 West	1993	730
01-0108	SPS-1	AC over BB	Rural Principal Arterial	US 280 West	1993	730
01-0109	SPS-1	AC over BB	Rural Principal Arterial	US 280 West	1993	730
01-0110	SPS-1	AC over BB	Rural Principal Arterial	US 280 West	1993	730
01-0111	SPS-1	AC over BB	Rural Principal Arterial	US 280 West	1993	730
01-0112	SPS-1	AC over BB	Rural Principal Arterial	US 280 West	1993	730
01-0161	SPS-1	AC over BB	Rural Principal Arterial	US 280 West	1993	730
01-0162	SPS-1	AC over BB	Rural Principal Arterial	US 280 West	1993	730
01-0163	SPS-1	AC over BB	Rural Principal Arterial	US 280 West	1993	730

SHRP_ID	Experiment	Pav. Structure*	Functional Class	Route	Const. Year	AADTT
01-0502	SPS-5	AC over UB	Rural Principal Arterial	US 84 East	1975	388
01-0503	SPS-5	AC over UB	Rural Principal Arterial	US 84 East	1975	388
01-0504	SPS-5	AC over UB	Rural Principal Arterial	US 84 East	1975	388
01-0505	SPS-5	AC over UB	Rural Principal Arterial	US 84 East	1975	388
01-0506	SPS-5/GPS-6S	AC+ AC over UB	Rural Principal Arterial	US 84 East	1975/2013	388
01-0507	SPS-5	AC over UB	Rural Principal Arterial	US 84 East	1975	388
01-0508	SPS-5	AC over UB	Rural Principal Arterial	US 84 East	1975	388
01-0509	SPS-5	AC over UB	Rural Principal Arterial	US 84 East	1975	388
01-0563	SPS-5/GPS-6S	AC + AC over UB	Rural Principal Arterial	US 84 East	1975/2013	388
01-0564	SPS-5	AC over UB	Rural Principal Arterial	US 84 East	1975	388
01-1001	GPS-1/GPS-6B	AC + AC over UB	Rural Principal Arterial	US 431 North	1980/1993	429
01-1011	GPS-2	AC over BB	Rural Minor Arterial	State 20 West	1985	179
01-1019	GPS-2/GPS-6S	AC + AC over BB	Rural Principal Arterial	US 43 South	1986/1998	370
01-1021	GPS-2	AC over BB	Rural Minor Arterial	State 14 West	1985	269
01-4073	GPS-2	AC over BB	Rural Principal Arterial	US 72 East	1988	399
01-4125	GPS-2	AC over BB	Urban Principal Arterial	State 152 West	1972	409
01-4126	GPS-1	AC over UB	Rural Principal Arterial	Interstate 65 South	1988	2208
01-4127	GPS-1/GPS-6B	AC + AC over UB	Rural Principal Arterial	US 72 East	1974/1989	256
01-4129	GPS-1/GPS-6B	AC + AC over UB	Rural Principal Arterial	US 280 East	1976/1989	431
01-4155	GPS-1/GPS-6S	AC + AC over UB	Rural Principal Arterial	US 84 East	1975/1999	242
01-6012	GPS-6A	AC + AC over BB	Rural Principal Arterial	Interstate 20 North	1984/1998	2524
01-6019	GPS-6	AC + AC over BB	Rural Principal Arterial	Interstate 65 North	1981/1994	1507
01-A320	SPS-3	AC over UB	Rural Principal Arterial	State 152 West	1972	634
01-A330	SPS-3	AC over UB	Rural Principal Arterial	State 152 West	1972	634
01-A340	SPS-3	AC over UB	Rural Principal Arterial	State 152 West	1972	634
01-A350	SPS-3	AC over UB	Rural Principal Arterial	State 152 West	1972	634
01-B310	SPS-3	AC + AC over UB	Rural Principal Arterial	US 43 South	1986	225
01-B320	SPS-3	AC over UB	Rural Principal Arterial	US 43 South	1986	225
01-B330	SPS-3	AC over UB	Rural Principal Arterial	US 43 South	1986	225
01-B340	SPS-3	AC over UB	Rural Principal Arterial	US 43 South	1986	225
01-B350	SPS-3	AC over UB	Rural Principal Arterial	US 43 South	1986	225
01-C310	SPS-3	AC + AC over UB	Rural Principal Arterial	US 84 East	1975	367
01-C320	SPS-3	AC over UB	Rural Principal Arterial	US 84 East	1975	367
01-C330	SPS-3	AC over UB	Rural Principal Arterial	US 84 East	1975	367
01-C340	SPS-3	AC over UB	Rural Principal Arterial	US 84 East	1975	367

SHRP_ID	Experiment	Pav. Structure*	Functional Class	Route	Const. Year	AADTT
01-C350	SPS-3	AC over UB	Rural Principal Arterial	US 84 East	1975	367

*AC = Asphalt Concrete; UB = Unbound Base; and BB = Bound Base

Table 6. Selected LTPP Sections in the Neighboring States

State	SHRP ID	Experiment	Pav. Structure	Functional Class	Const. Year	AADTT
FL	12-4096	GPS-2/ GPS-6C	AC + AC over BB	Rural Principal Arterial	1987/2003	14/116
	12-4097	GPS-2	AC over BB	Rural Principal Arterial	1987	1062
	12-4100	GPS-2/ GPS-6S	AC + AC over BB	Urban Principal Arterial	1987/2002/ 2012	93/105/125
	12-4108	GPS-2/ GPS-6S	AC + AC over BB	Rural Minor Arterial	1987	145
GA	13-0502	SPS-5	AC over UB	Rural Principal Arterial	1987/1993	5335
	13-0503	SPS-5	AC over UB	Rural Principal Arterial	1987/1993	5335
	13-0504	SPS-5	AC over UB	Rural Principal Arterial	1987/1993	5335
	13-0505	SPS-5	AC over UB	Rural Principal Arterial	1987/1993	5335
	13-0506	SPS-5	AC over UB	Rural Principal Arterial	1987/1993	5335
	13-0507	SPS-5	AC over UB	Rural Principal Arterial	1987/1993	5335
	13-0508	SPS-5	AC over UB	Rural Principal Arterial	1987/1993	5335
	13-0509	SPS-5	AC over UB	Rural Principal Arterial	1987/1993	5335
	13-0560	SPS-5	AC over UB	Rural Principal Arterial	1987/1993	5335
	13-0561	SPS-5	AC over UB	Rural Principal Arterial	1987/1993	5335
	13-0562	SPS-5	AC over UB	Rural Principal Arterial	1987/1993	5335
	13-0563	SPS-5	AC over UB	Rural Principal Arterial	1987/1993	5335
	13-0564	SPS-5	AC over UB	Rural Principal Arterial	1987/1993	5335
	13-0565	SPS-5	AC over UB	Rural Principal Arterial	1987/1993	5335
	13-0566	SPS-5	AC over UB	Rural Principal Arterial	1987/1993	5335
	13-4096	GPS-2/ GPS-6C	AC + AC over BB	Rural Minor Collector	1987/2001	46/167
	13-4119	GPS-2	AC over BB	Rural Principal Arterial	1987/1993	6842
MS	28-1001	GPS-2/ GPS-6S	AC + AC over BB	Rural Principal Arterial	1987/1998/ 2002	178/913
	28-3081	GPS-2/ GPS-6S	AC + AC over BB	Rural Principal Arterial	1987/1990/ 1996	290/1717
	28-3091	GPS-2/ GPS-6S	AC + AC over BB	Rural Principal Arterial	1987/1995	280/284
	28-3093	GPS-2/ GPS-6S	AC + AC over BB	Rural Principal Arterial	1987/1989	1063/1494
	28-3094	GPS-2/ GPS-6B	AC + AC over BB	Rural Principal Arterial	1987/1989	1063/1497
TN	47-1029	GPS-2/ GPS-6S	AC + AC over BB	Rural Principal Arterial	1987/1998/ 2014	70/237/1184

Figure 6 shows the LTPP asphalt pavement sections in Alabama and its neighboring states, namely GA, MS, TN, and the Florida panhandle in the LTPP InfoPave™. The LTPP test locations in the red boundary line in Figure 6 comprise the 51 LTPP sections within Alabama and those neighboring states closest to Alabama's state line.

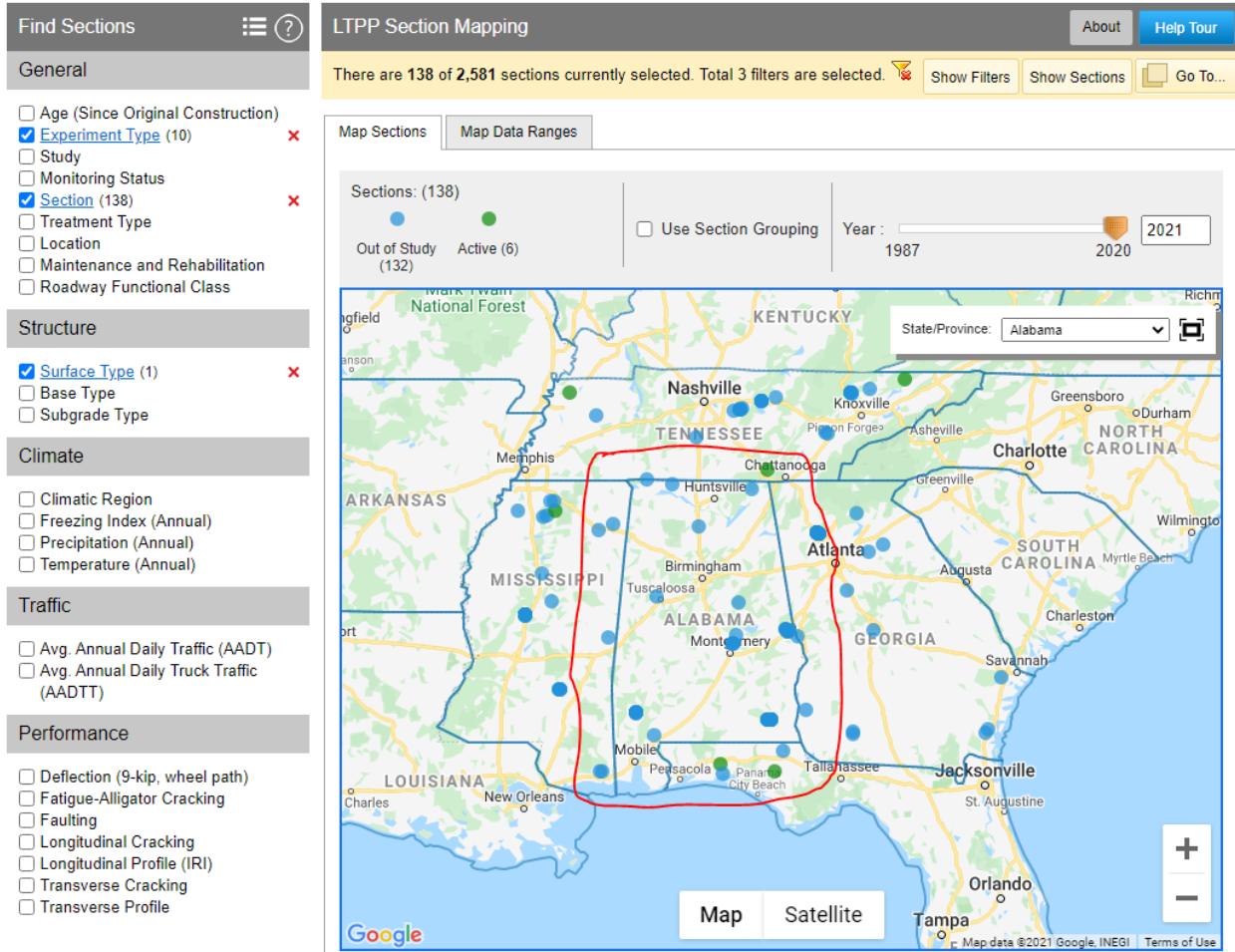


Figure 6. LTPP Sections in Alabama and Neighboring States Selected for Local Verification

3.3.1 LTPP Traffic Inputs

Traffic data is a critical input parameter in the design and analysis of pavement structures. In the 1193 AASHTO Design Guide, traffic data are processed to convert the entire traffic loading into 18-kip Equivalent Single Axle Loads (ESALs) using AASHTO equivalency factors. However, PMED follows a more comprehensive method for characterizing highway traffic loading, which uses Normalized Axle Load Spectra (NALS) for each axle type in each vehicle class. These data can be collected from Weigh-In-Motion (WIM) stations (Prozzi & Hong, 2006).

NALS are percentile distributions of axle counts by load level, calculated for each axle type and for each vehicle or truck class. The axle types used in the PMED software include single, tandem, tridem, and quad axles. In addition, the vehicle classes used in the PMED software range from Class 4 to 13, as illustrated in Figure 7 (FHWA, 2013).

















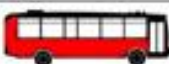

















Class 1 Motorcycles		Class 7 Four or more axle, single unit	
Class 2 Passenger cars		Class 8 Four or less axle, single trailer	
			
			
			
Class 3 Four tire, single unit		Class 9 5-Axle tractor semitrailer	
			
			
Class 4 Buses		Class 10 Six or more axle, single trailer	
			
		Class 11 Five or less axle, multi trailer	
Class 5 Two axle, six tire, single unit		Class 12 Six axle, multi-trailer	
			
		Class 13 Seven or more axle, multi-trailer	
Class 6 Three axle, single unit			
			
			

Figure 7. FHWA Vehicle Classification (FHWA, 2013)

Table 7 summarizes the hierarchical levels for traffic inputs used in the PMED analysis of the LTPP test sections, as executed using the PMED software for this study. The Annual Average Daily Truck Traffic (AADTT) with a Level 1 input represents the initial AADTT for the specific roadway segment. Similarly, the number of lanes, vehicle class distribution and growth, and NALS are all considered Level 1 design inputs. The Monthly Adjustment Factor (MAF), representing the fractional distribution of the yearly AADTT across vehicle classes, is assigned a Level 3 input in this study. The same Level 3 input level applies to other PMED software traffic parameters, including axle configuration, lateral wander, and wheelbase.

Table 7. Traffic Input Levels

Design Input	LTPP Sheet Name	Input Level
AADTT	MEPDG_TRUCK_VOL_PARAMETERS	Level 1
No. of Lanes	SHRP_INFO	Level 1
Axle Configuration	Default	Level 3
Lateral wander	Default	Level 3
Wheelbase	Default	Level 3
Veh. Class Distr. & Growth	MEPDG_TRUCK_VOL_PARAMETERS	Level 1
Monthly Adjustment	Default	Level 3
Axles Per Truck	MEPDG_AXLE_PER_TRUCK	Level 1

3.3.2 Pavement Structure Inputs

The pavement structure inputs for LTPP sections include the layer thicknesses and their material properties. As previously discussed, the prevalent layer types of the LTPP sections considered in this study are Asphalt Concrete (AC) overlays (i.e., AC + AC over Unbound Granular Base (UB) and AC + AC over Bound Base (BB)), AC over UB, and AC over BB.

Some LTPP sections with AC overlays had more than four AC layers, complicating their analysis in the PMED software. In some cases, the additional AC overlayer was less than 1 inch thick, so it was modeled in the PMED software by combining the thin AC layer's thickness with the milled AC surface layer. Thus, the total thicknesses of modeled pavement structures were the same as the overall thickness of the LTPP sections with fewer layers. This approach aligns with that of Islam (2019) following the Kansas Department of Transportation's (KDOT) suggestions. The underlying assumption is that the properties of such thin AC layers do not notably affect performance predictions of the analyzed LTPP sections.

Table 8 summarizes the thickness and material property inputs required for the PMED analysis. Most inputs are at Level 1, except for creep compliance, base resilient modulus, and subgrade resilient modulus. For LTPP overlay sections, back-calculated resilient moduli were used for existing AC layers and the underlying layers, including the base, subbase, and subgrade. In some cases where dynamic modulus data were missing, the Artificial Neural Networks for Asphalt Concrete Dynamic Modulus ($|E^*|$) Prediction (ANNACAP) tool from the LTPP InfoPave™ website was employed. This tool utilizes Artificial Neural Network (ANN) models to yield accurate and

reliable dynamic modulus predictions for asphalt concrete at specific temperatures and loading frequencies. The ANN models can also be utilized to evaluate the $|E^*|$ and develop a master curve. These models were developed by Kim et al. (2011a) utilizing the data in the LTPP database.

Table 8. Pavement Structure Input Levels

Design Input	LTPP Sheet Name	Input Level
Thickness	TST_L05B	1
Pavement Layer Classifier/ Material Type	TST_L05B/ TST_SS04_UG08/ TST_TB01	1
Air Voids	TST_AIR_VOIDS_SECT	1
Effective Binder Content	TST_AC04/ TST_AC03/ TST_AE03	1
Aggregate Gradation (AC Layer)	TST_AG04	1
Poisson	TST_AC07_V2_MR_SUM	1
Asphalt Binder	TST_AE05 & TST_AE03	1
Dynamic Modulus	TST_ESTAR_MODULUS	1
Kinematic & Absolute Viscosity	TST_AE05	1
Base & Subgrade Gradation	TST_SS01_UG01_UG02	1
Moisture Content (subgrade & Base)	TST_UG10_SS09	1
Liquid & Plasticity Limit	TST_UG04_SS03	1
Design & Traffic Date	Basic Section Overview	1
Creep Compliance	TST_AC07_V2_CREEP_COMP_SUM	2
Base Resilient Modulus	BAKCAL_MODULUS_SECTION_LAYER	2
Subgrade Resilient Modulus	BAKCAL_MODULUS_SECTION_LAYER	2

Figure 8 illustrates the hierarchical distribution of various $|E^*|$ prediction models available in the ANNACAP tool. If available, the most accurate $|E^*|$ predictions can be achieved for an asphalt mixture using the resilient modulus (MR) data. Conversely, if only binder grade and volumetric properties (i.e., VV-Grade) were reported for a mixture in the LTPP database, these can still be used for predictions. However, the VV-Grade data typically yield less accurate $|E^*|$ predictions.

For example, the ANNACAP tool was used to generate the $|E^*|$ data for LTPP Section 01-4127 using the VV-grade prediction model due to limited available data. The binder grade and volumetric properties data of LTPP Section 01-4127 served as the input parameters for the VV-grade prediction model. Figure 9 provides a screenshot of the prediction model input for LTPP Section 01-4127, and Table 9 summarizes the output.

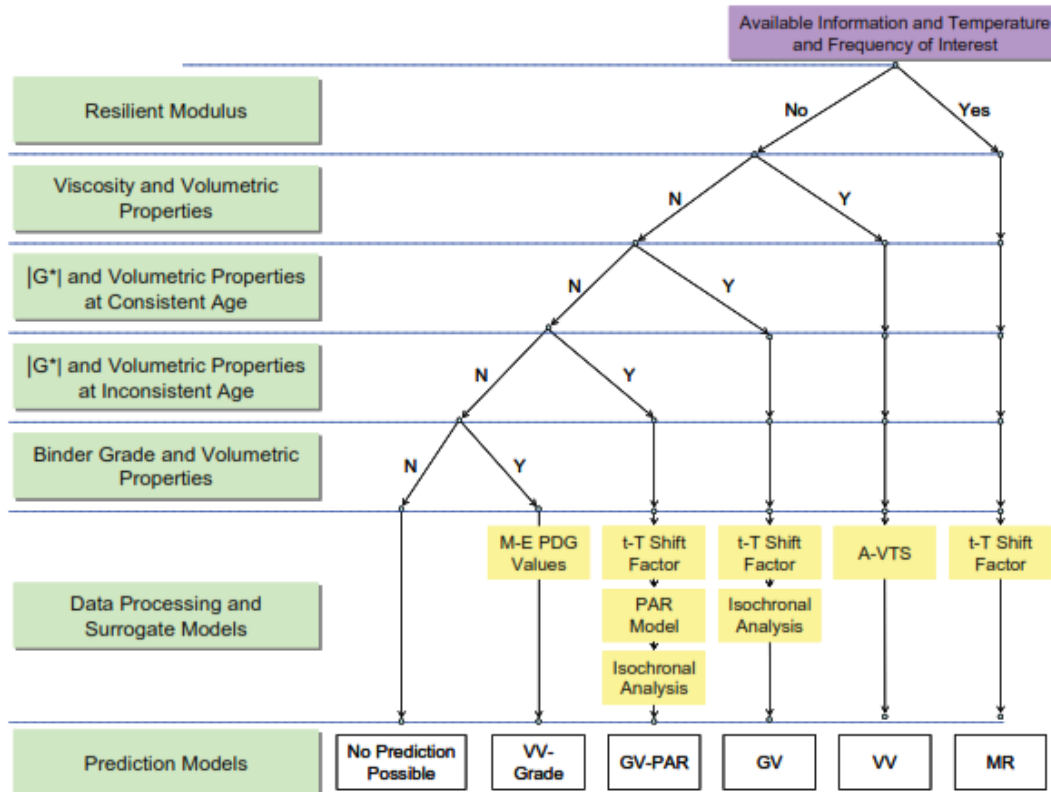


Figure 8. Hierarchy of Dynamic Modulus Prediction Models (Kim et al., 2011b)

The screenshot shows the 'Input Parameters' window in the ANNACAP software. The window is divided into two main sections: 'Layer ID' and 'Model'. The 'Layer ID' section includes fields for State Code (01), Project ID (4127), Project Layer (6), Construction Date (08-Aug-89), and Aging Level (RTFO/TFO). The 'Model' section includes a dropdown for 'Model to Use' (Viscosity Based ANN), a dropdown for 'Analysis Level' (Level 3), and input fields for VMA (15) and VFA (75). The right side of the window shows the 'Binder Grade' (AC-20) and input fields for 'A' (10.7709) and 'VTS' (-3.6017).

Figure 9. Screenshot of Input Data for LTPP Section 01-4127 in ANNACAP

Table 9. ANNACAP |E*| Prediction for LTPP Section 01-4127

State Code	Project_ID	Project Layer	Const. Date	Sample Type	Predictive Model	Temperature (°F)	Frequency (Hz)	Predicted E* _(psi)
1	4127	6	8-Jun-89	2	VV-Grade	14	25.0	4,392,665
1	4127	6	8-Jun-89	2	VV-Grade	14	10.0	4,304,568
1	4127	6	8-Jun-89	2	VV-Grade	14	5.0	4,198,818
1	4127	6	8-Jun-89	2	VV-Grade	14	1.0	3,842,762
1	4127	6	8-Jun-89	2	VV-Grade	14	0.5	3,688,187
1	4127	6	8-Jun-89	2	VV-Grade	14	0.1	3,177,665
1	4127	6	8-Jun-89	2	VV-Grade	40	25.0	3,983,040
1	4127	6	8-Jun-89	2	VV-Grade	40	10.0	3,883,345
1	4127	6	8-Jun-89	2	VV-Grade	40	5.0	3,770,269
1	4127	6	8-Jun-89	2	VV-Grade	40	1.0	3,403,650
1	4127	6	8-Jun-89	2	VV-Grade	40	0.5	3,230,691
1	4127	6	8-Jun-89	2	VV-Grade	40	0.1	2,609,466
1	4127	6	8-Jun-89	2	VV-Grade	70	25.0	1,809,784
1	4127	6	8-Jun-89	2	VV-Grade	70	10.0	1,616,601
1	4127	6	8-Jun-89	2	VV-Grade	70	5.0	1,451,864
1	4127	6	8-Jun-89	2	VV-Grade	70	1.0	1,034,180
1	4127	6	8-Jun-89	2	VV-Grade	70	0.5	891,588
1	4127	6	8-Jun-89	2	VV-Grade	70	0.1	538,907
1	4127	6	8-Jun-89	2	VV-Grade	100	25.0	578,941
1	4127	6	8-Jun-89	2	VV-Grade	100	10.0	449,981
1	4127	6	8-Jun-89	2	VV-Grade	100	5.0	368,697
1	4127	6	8-Jun-89	2	VV-Grade	100	1.0	214,226
1	4127	6	8-Jun-89	2	VV-Grade	100	0.5	173,263
1	4127	6	8-Jun-89	2	VV-Grade	100	0.1	91,549
1	4127	6	8-Jun-89	2	VV-Grade	130	25.0	165,589
1	4127	6	8-Jun-89	2	VV-Grade	130	10.0	127,403
1	4127	6	8-Jun-89	2	VV-Grade	130	5.0	102,585
1	4127	6	8-Jun-89	2	VV-Grade	130	1.0	57,817
1	4127	6	8-Jun-89	2	VV-Grade	130	0.5	47,796
1	4127	6	8-Jun-89	2	VV-Grade	130	0.1	29,758

3.3.3 Climatic Inputs

Climate plays a pivotal role in the performance of asphalt pavements. Specifically, the performance of unbound layers in asphalt pavement is affected by moisture content (Kim et al., 2011a; Islam, 2019). In addition, the performance of bound layers, such as asphalt concrete, is largely affected by temperature fluctuations over their service life.

The PMED software utilizes data from two key sources—Modern-era Retrospective-analysis for Research and Applications (MERRA) and North American Regional Reanalysis (NARR)—to acquire hourly climate data. This data includes temperature, precipitation, wind speed, relative humidity, and cloud cover for a chosen weather station. This information is considered in the pavement design and analysis through the Enhanced Integrated Climatic Model (EICM), embedded within the PMED software. EICM assesses the impacts of moisture and temperature on roadway segments by simulating changes in pavement material properties over time.

Weather stations for any state in the United States can be accessed directly from the PMED software interface. Users can enter the state name, as depicted in Figure 11. When a desired weather station is unavailable in the PMED software, weather data can be retrieved by clicking on a specific weather station, which opens a link to the InfoPave™ MERRA data page. Inputting the geographic coordinates of the weather station in the 'Search Location' bar on this page returns an icon for that specific weather station on the map. Users can click on this icon and subsequently on the 'Download MERRA Climate Data File' to download the .hcd file to a specified directory on the local machine. This .hcd file must then be downloaded or transferred to the PMED program data's .hcd folder on the local machine to activate the weather station data in the PMED software. It is important to note that for PMED analysis, the PMED software only requires selecting a weather station closest to the geographic coordinates of the roadway segment under consideration.

Furthermore, the PMED software requires inputting the depth of the water table as part of the project's climate information. For LTPP sections in Alabama, a groundwater table depth of 6 feet was selected based on data from the Natural Resource Conservation Service (NRCS) soil database (NRCS, 2021).

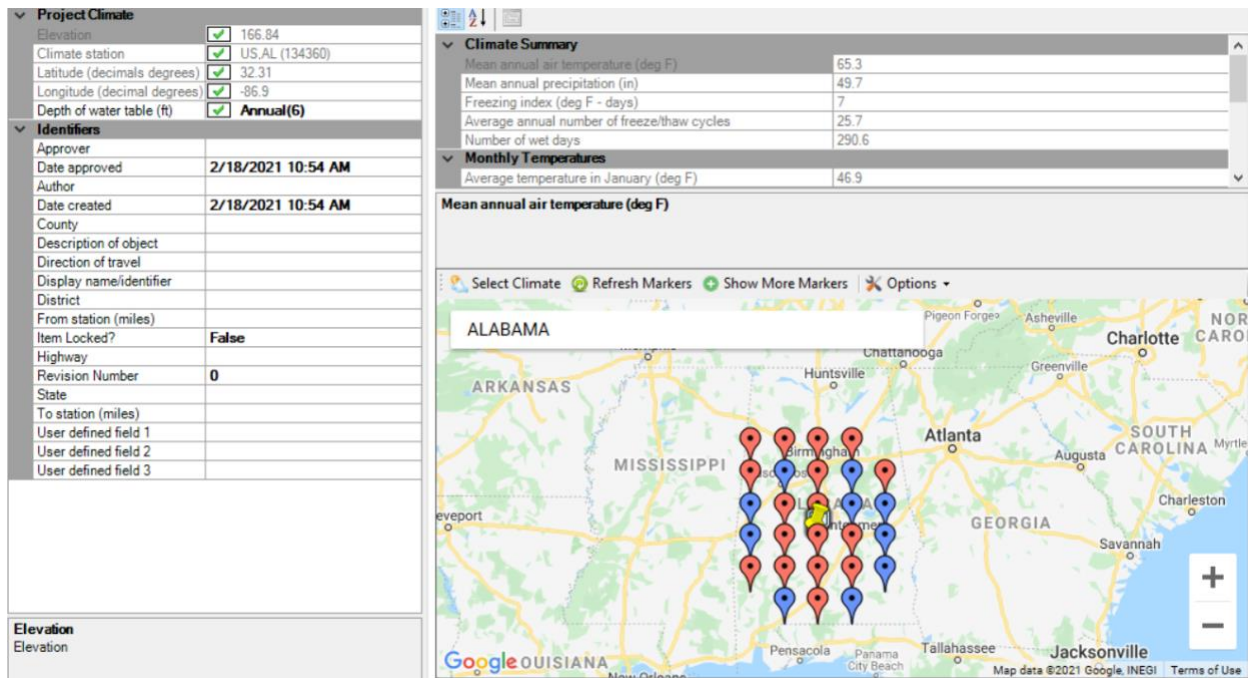


Figure 10. Weather Stations in Alabama

3.4 Data for NCAT Test Track Sections

In addition to the data from the LTPP test sections in Alabama and those close to the Alabama state line in adjacent states, this study also utilized data collected from the structural pavement experiments conducted on the NCAT Test Track in five research cycles (i.e., 2003, 2006, 2009, and 2012).

The NCAT Test Track in Opelika, Alabama, is a full-scale APT facility with truck traffic. The 1.7-mile oval track consists of 46 individual test sections, each spanning 200 feet. Of these, 26 sections are on the track's straight segments, while 20 are on the curves. The NCAT Test Track operates on a three-year cycle, including a 6-month construction or replacement phase for existing sections. This is followed by a 2-year period during which the test sections on the track are applied with approximately 10 million Equivalent Single Axle Loads (ESALs). A subsequent forensic analysis evaluates the observed distresses in test sections.

Prior to initiating each research cycle, the component materials undergo testing, and asphalt mixtures are designed. For the structural pavement experiments, performance tests are also carried out for pavement design and analysis to plan the experiments. During the construction of the test sections, plant mixtures are sampled for quality control and future performance testing, facilitating a comprehensive characterization of mechanistic and performance properties of the asphalt mixtures evaluated in the experiments. During the 2-year loading period, the field performance of each test section is monitored on a weekly basis using an automated pavement distress data collection vehicle to quantify pavement smoothness and distresses. The test sections for the structural pavement experiments are also instrumented with strain sensors and

pressure plates that capture the dynamic response of the pavement under traffic loads (Timm 2009).

The subsequent sub-sections describe the data from the NCAT Test Track's structural pavement experiments across the five research cycles (Guo, 2015), serving as key inputs for local verification in this study.

3.4.1 Traffic Inputs

The test sections on the NCAT Test Track are subjected to approximately 10 million ESALs over a period of around two years. A fleet of five trucks applies this traffic loading, each truck weighing approximately 156,995 pounds. The fleet operates in two shifts from Tuesday through Saturday. To accommodate data collection activities, including the measurement of rutting, the assessment of ride quality, and the mapping of surface cracks, traffic is suspended every Monday. Given the controlled schedule for truck traffic throughout the research cycle, neither an increase in traffic volume nor a yearly growth rate is observed.

3.4.2 Pavement Structures and Material Inputs

A total of 31 structural experiment sections, spanning the 2003, 2006, 2009, and 2012 research cycles, were selected for local verification in this study. These sections were specifically selected because they were newly constructed within their respective research cycles. This is essential for enabling continuous traffic modeling in the PMED software, which is not capable of bridging the one-year gaps between research cycles required for construction and forensic investigation.

- 2003 research cycle: 8 sections (N1 through N8)
- 2006 research cycle: 6 sections (N1, N2, N8, N9, N10 and S11)
- 2009 research cycle: 10 sections (N5, N6, N7, N10, N11, S8, S9, S10, S11 and S12)
- 2012 research cycle: 7 sections (N3, N4, S12, N5, S5, S6 and S13)

Figure 11 shows the structural experiment sections from the 2003 NCAT Test Track research cycle, all of which were newly constructed and thus selected for local calibration in this study. These test sections were built on the same subgrade, classified as A-4(0) (i.e., Track Soil), and a 6-inch crushed aggregate base course. However, the asphalt structure of each test section varied (Guo, 2015):

- Sections N1 through N6 had a pairwise configuration, with each pair having the same asphalt structure thickness. Within each pair, one section was constructed with an unmodified asphalt binder (i.e., PG 67-22), while the other was built with a modified asphalt binder (i.e., PG 76-22).
- Sections N7 and N8 shared the same asphalt structure thickness. They also had the same Stone Matrix Asphalt (SMA) surface with a modified binder (i.e., PG 76-22) and the same binder layer mixture with an unmodified binder (i.e., PG 67-22). However, the base layer mixture in Section N8 had an extra 0.5% asphalt binder (i.e., rich bottom layer).

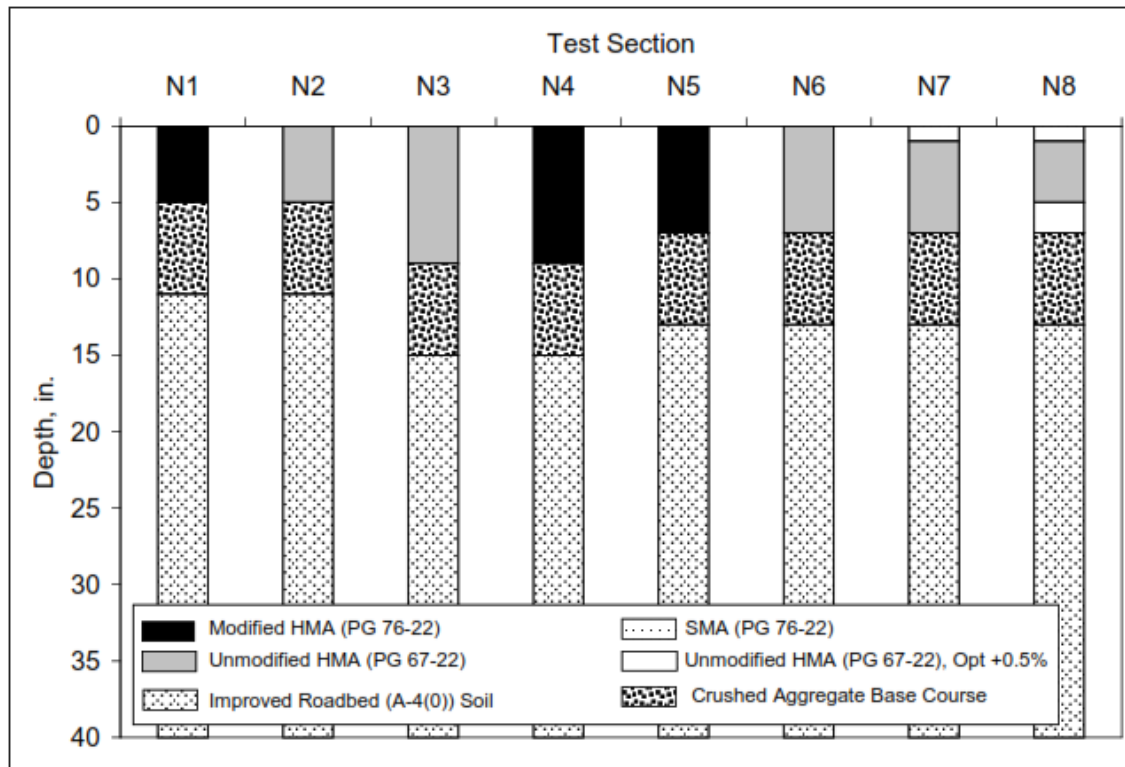


Figure 11. Structural Sections of the 2003 Test Track Cycle (Timm & Priest, 2006)

The 2006 test track research cycle comprised 11 structural experiment sections, six of which were selected for this local verification study. Although Sections N3 to N7 remained structurally sound following the 2003 research cycle, they were not included in this study due to a discontinuity in traffic application between the 2003 and 2006 research cycles. The one-year gap was reserved for forensic investigation and the maintenance, reconstruction, or rehabilitation of test sections in preparation for the subsequent cycle. Such discontinuities present challenges for modeling in the PMED software. Figure 12 illustrates the structural sections from the 2006 research cycle, highlighting the six newly constructed sections chosen for this study. A brief overview of these selected structural experiment sections follows:

- Sections N1 and N2, sponsored by the Florida DOT, were built atop a 10-inch limerock base course. Section N1 had three lifts of asphalt mixture with an unmodified asphalt binder (i.e., PG 67-22), whereas Section N2 had an asphalt base course with an unmodified binder (i.e., PG 67-22) and two upper lifts using an SBS-modified PG 76-22 binder.
- Sections N8 and N9, sponsored by the Oklahoma DOT, differed in thickness. Section N8 had 10 inches of AC, while Section N9 featured 14 inches of AC. Both had a PG 76-28 SMA surface course, a PG 76-28 upper binder course, a PG 64-22 lower binder course, and a PG 64-22 base lift designed at 2% air voids to yield a higher binder content for enhanced bottom-up fatigue resistance. Section N9 had an extra PG 64-22 lower binder lift.

- Section N10, sponsored by the Missouri DOT, was constructed on a dolomitic limerock base course, classified as Missouri Type 5 aggregate base. The asphalt structure had three layers, including a surface and upper binder layer, both using a PG 70-22 binder course and a lower binder course with a PG 64-22 binder.
- Section S11, funded by the Alabama DOT, comprised two upper asphalt lifts with a modified PG 76-22 binder and two lower asphalt lifts using an unmodified PG 67-22 binder.

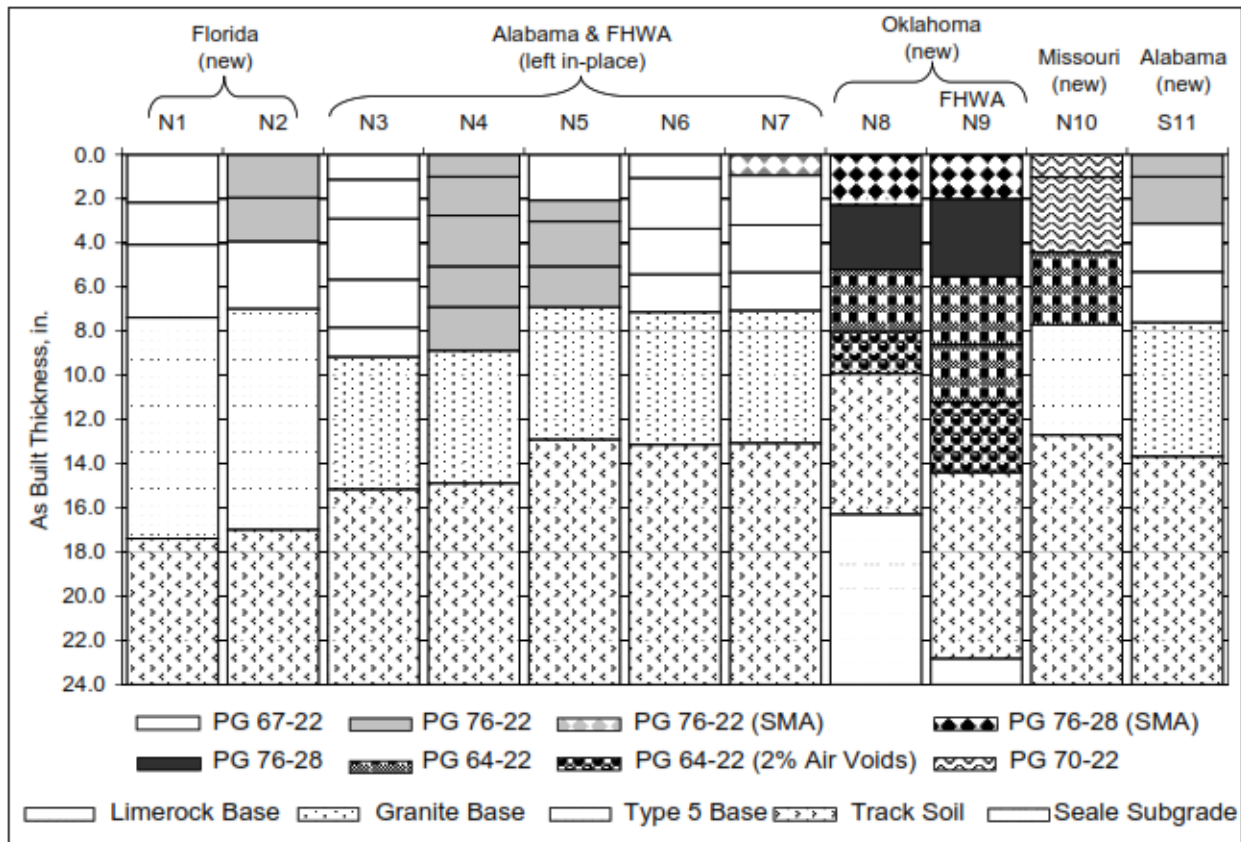


Figure 12. Structural Sections of the 2006 Test Track Cycle (Timm, 2009)

The 2009 research cycle encompassed 16 structural experiment sections. Of these, Sections N1, N2, N8, and N9 originated from the 2006 research cycle, while Sections N3 and N4 were carried over from the 2003 research cycle. These sections received minimal or no maintenance and were left in place. As previously discussed, the discontinuity in traffic application made these older sections difficult to model in the PMED software for this local verification study.

In the 2009 research cycle, 10 newly constructed structural experiment sections (i.e., N5–N7, N10, N11, and S8–S12) were selected for this local verification study, as shown in Figure 13. The asphalt structures of these selected sections are as follows:

- Sections N5 and N6 were sponsored by Shell and utilized Thiopave technology, involving sulfur as a partial binder replacement in the asphalt mixture to mitigate the rising costs

of virgin asphalt binders. Section N5 had an AC thickness of 9 inches and comprised a PG 76–22 wearing course, two lifts of 40% Thiopave asphalt mixture, and a base lift with 30% Thiopave asphalt mixture. Section N6, which was 7 inches thick, had a similar asphalt structure but included only one lift of 40% Thiopave asphalt mixture.

- Section N7 was sponsored by Kraton to evaluate a new highly polymer-modified asphalt binder. Section N7 was only 5.75 inches thick and composed three lifts of Kraton’s highly polymer-modified asphalt (HiMA) mixture.
- The remaining structural experiment sections included in this local verification study were from a group experiment to evaluate the performance and structural contribution of the asphalt mixtures with 50% Recycled Asphalt Pavement (RAP) and different warm mix asphalt (WMA) technologies. Section S9 served as the control and was constructed with a virgin asphalt mixture. Sections N10 and N11 included high RAP mixtures (i.e., 50% RAP) produced as hot mix and warm mix, respectively. Section S8 featured an open-graded friction course (OGFC) surface layer, an intermediate lift of PG 67–22 asphalt mixture, and a base lift of PG 76–22 asphalt mixture. Sections S10 and S11 were built with virgin warm mixes. Section S10 utilized asphalt binder foaming, while Section S11 used a chemical additive. Lastly, Section S12 was sponsored by Lake Asphalt of Trinidad and Tobago Ltd and utilized 25% Trinidad Lake Asphalt (TLA) pellets in its asphalt layers.

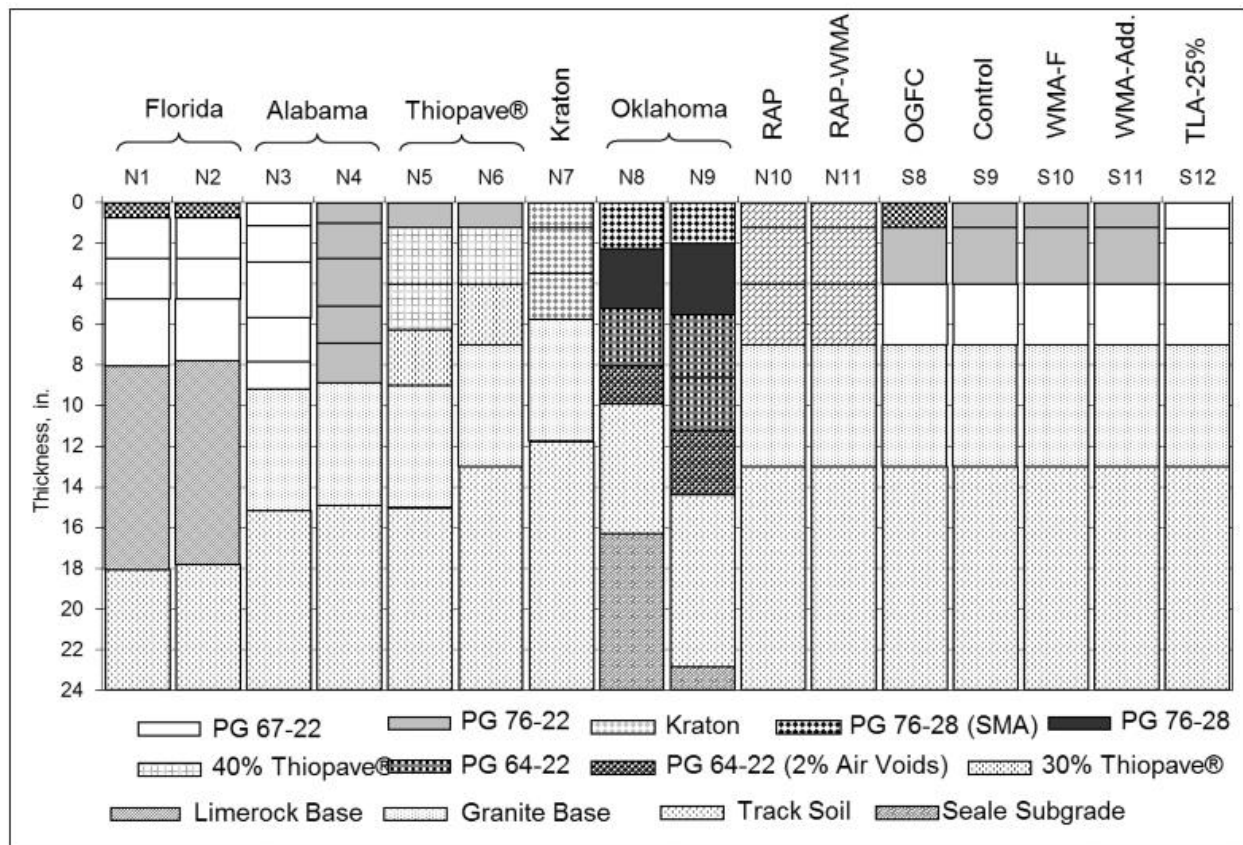


Figure 13. Structural Sections of the 2009 Test Track Cycle (Courtesy of David Timm)

The 2012 research cycle included 16 structural experiment sections, of which seven newly built sections, including N3, N4, N5, S5, S6, S12, and S13, were selected for this local verification study. The selected structural experiment sections shared the same subgrade material (i.e., track soil) and crushed aggregate base. Figure 14 illustrates the pavement structures of these seven sections with further details as follows:

- Sections N3, N4, and S12 were sponsored by the Virginia DOT and built using Cold Central Plant Recycling (CCPR) technology for the base lift of the asphalt structures. Section N3 featured a granular base and four lifts of asphalt, including an SMA surface lift, two intermediate Virginia Superpave asphalt mixture lifts, and a CCPR bottom lift using foamed asphalt. Section N4 had a similar asphalt structure but included only one intermediate Virginia Superpave lift. Section S12 was built with a Full Depth Reclamation (FDR) base and had three lifts of asphalt: an SMA surface course, an intermediate Virginia Superpave lift, and a bottom lift of foamed CCPR.
- Sections N5, S5, S6, and S13 were part of the Green Group (GG) experiment, which was named based on the material composition of the asphalt mixtures used in this experiment. They were built with 6 inches of asphalt mixtures. Section N5 was the control section with the maximum RAP contents permitted by state highway agencies. Section N5 consisted of a PG 67–22 surface course with 20% RAP and intermediate and bottom lifts with a PG 67–22 binder and 35% RAP. Section S5 was a high RAP section. It had an SMA surface with a PG 67-22 binder and 25% RAP, an intermediate lift with a PG 67-22 binder and 50% RAP, and a bottom layer with a HiMA (PG 94-28) binder and 35% RAP. Section S6 was a RAP and Recycled Asphalt Shingles (RAS) section. It encompassed a SMA surface layer with a PG 67-22 binder and 5% RAS and an intermediate layer with a PG 67-22 binder, 25% RAP, and 5% RAS. The bottom lift of Section S6 contained a PG 76-22 binder and 25% RAP and was designed with 2% design air voids as a rich-bottom layer to make it more fatigue-resistant. Lastly, Section S13 was a ground tire rubber (GTR) section featuring two GTR modified binders: one contained 12% #30-mesh GTR added to a PG 67-22 (ARB12), and the other contained 20% #16-mesh GTR added to a PG 67-22 (ARB20). ARB12 was utilized in the SMA surface and the 35% RAP intermediate lift, while ARB20 was used in the Arizona gap-graded bottom layer (ARB20 AZ).

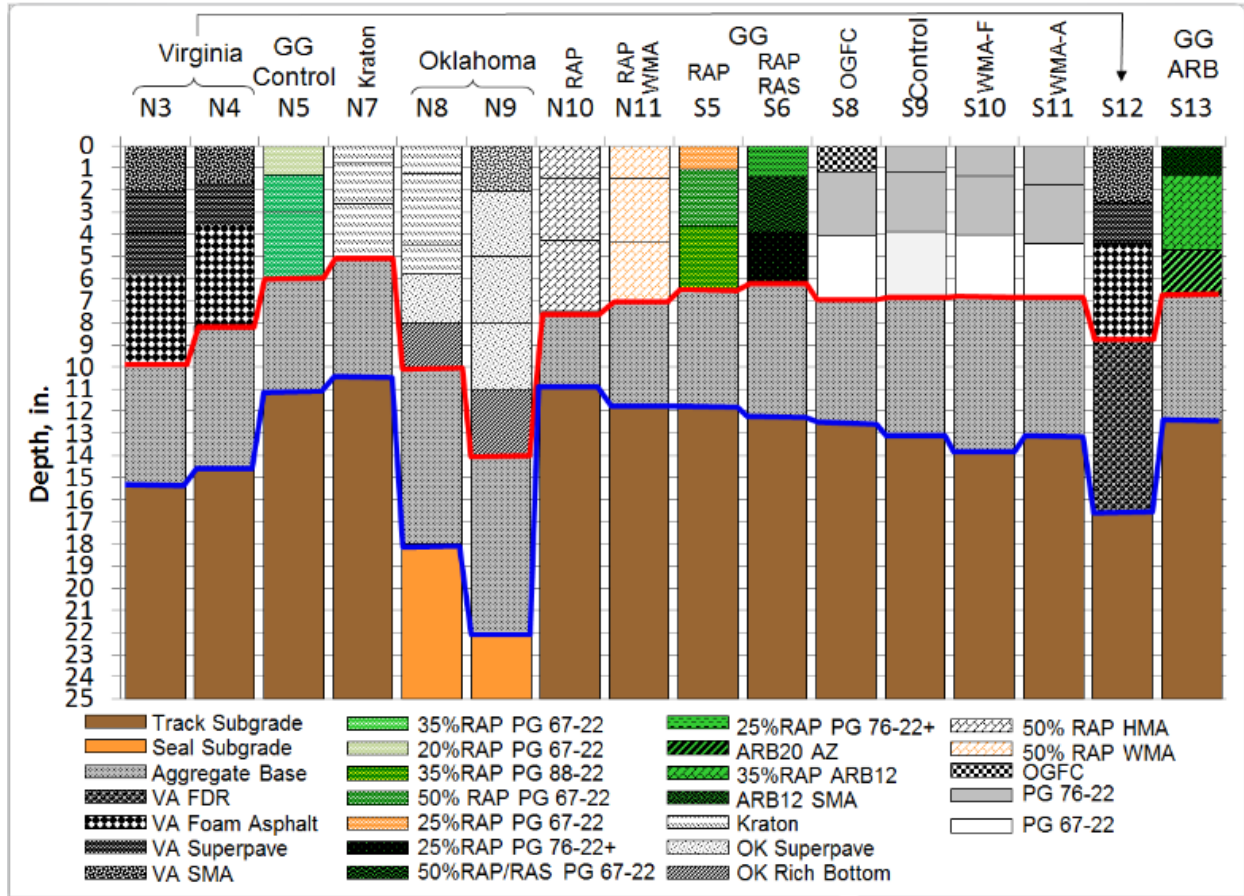


Figure 14. Structural Sections of the 2012 Test Track Cycle (Courtesy of David Timm)

Key material inputs for the Test Track structural experiment sections encompass dynamic moduli (E^*) and binder properties for the asphalt mixtures, as well as resilient moduli (M_R) for the base course and subgrade. The dynamic moduli for the selected structural experiment sections in this local verification study were determined by conducting the E^* testing on reheated, plant-produced asphalt mixes. For the 2003 asphalt mixtures, testing was conducted at Purdue University (Timm and Priest, 2006). The mixtures from the 2006, 2009, and 2012 research cycles underwent E^* testing at the NCAT laboratory, following the AASHTO TP 62-07 procedure (Robbins, 2013). Key asphalt binder properties, including the dynamic shear modulus (G^*) and phase angle (δ), were determined using the Dynamic Shear Rheometer (DSR) per AASHTO T315-06 at the NCAT laboratory (Guo, 2015).

Additionally, M_R values were also determined for the base course and subgrade at the NCAT Test Track. For the 2003 structural experiment sections, M_R was back-calculated using Falling Weight Deflectometer (FWD) deflection data. FWD is a non-destructive testing (NDT) method that evaluates the structural capacity of existing pavement by simulating pavement deflection due to truck traffic. The test involves dropping a known weight onto the pavement surface and measuring the resultant deflections, which are then used to back-calculate the pavement's structural capacity. For the 2006, 2009, and 2012 structural experiment sections, M_R was also

obtained through theoretical computations. These computations utilized vertical pressures in pavement layers and laboratory triaxial test results to generate representative moduli for each layer (Taylor and Timm, 2009; Guo, 2015).

3.4.3 Climate Characterization

The NCAT Test Track is in a humid subtropical climate zone characterized by seasonal variations: hot summers, warm autumns, mild winters, and early springs. To monitor these climatic conditions, a weather station has been installed in close proximity to the facility. As depicted in Figure 15, this station collects comprehensive weather data on an hourly basis, capturing variables such as the time of observation, temperature, solar energy levels, wind speed, precipitation rates, and relative humidity. Although the weather station provides valuable data, this study relies on the climatic information embedded in the PMED software rather than using the localized data from the Test Track's weather station.



Figure 15. Weather Station at NCAT Test Track

3.4.4 Field Performance Data

At the NCAT Test Track, key performance indicators such as surface roughness and critical pavement distresses—including rutting and cracking—are monitored on a weekly basis. Rut depth is quantified using the ALDOT beam procedure, detailed in the ALDOT T-392 standard specification. Figure 16 shows the ALDOT beam, a 4-foot beam equipped with a dial gauge. This apparatus measures total rut depths along predetermined wheel paths within each test section. The accuracy of these measurements is estimated at ± 2.5 mm. For evaluating ride quality, the IRI of each test section is measured using the Dynatest Mark IV inertial profiler, as shown in Figure 16.



Figure 16. ALDOT Beam (Left) and Inertial Profiler (R) (Giler, 2017)

Cracking performance is initially assessed through visual inspection of each test section. Observed surface cracks are subsequently mapped, as illustrated in Figure 17, and quantified through linear measurements within the designated test sections. These measurements are then used to calculate the percentage of lane area affected by cracking (Giler, 2017). In addition, core samples are extracted from selected test sections to identify the mode of cracking—either bottom-up or top-down—manifested in the pavement.



Figure 17. Crack Mapping at the Test Track (Giler, 2017)

CHAPTER 4 LOCAL VERIFICATION OF PMED PREDICTION MODELS

This chapter presents the local verification results of the PMED prediction models that have been globally calibrated, including distress and IRI models. It utilizes data from LTPP asphalt pavement sections in Alabama and neighboring states near Alabama's state line, as well as data from the NCAT Test Track. The analysis includes the bias and the standard error of estimate (S_e) of the prediction models.

4.1 Local Verification

Local verification of the globally calibrated prediction models in MEPDG is essential in the local calibration framework. The global calibration coefficients for the distress models are summarized in Table 10. The PMED software version 2.6 was used to predict distress and smoothness (IRI) for test sections using LTPP and NCAT Test Track data. The LTPP data includes general (LTPP) pavement sections and overlay (LTPP_OL) pavement sections, including those in SPS-5 and GPS-6 experiments. The LTPP and LTPP_OL pavement sections were evaluated separately as the overlay sections inherently having reflective cracking that was accounted for in the transverse and bottom-up fatigue cracking distress models.

The predictions were compared to field-measured data using a paired student's t-test at a 5% significance level to detect any model bias. The null hypothesis (H_0) of the statistical test indicates that no significant difference exists between the predicted and measured data. A 5% significance level equates to a 5% risk of concluding a significant difference (or bias). Additionally, the standard error of estimate (S_e), a measure of model precision, was assessed. Local verification analysis was carried out using an R script. The results of local verification are detailed in the subsequent sections.

Table 10. Global Calibration Coefficient of the Distress Prediction Models

Distress Model	Global Calibration Coefficient
Rutting (AC Layer)	$\beta_{r1} = 0.40, \beta_{r2} = 0.52, \beta_{r3} = 1.36$ $k_{r1} = 2.4545, k_{r2} = 3.01, k_{r3} = 0.22$
Rutting (Unbound Layer)	$\beta_{b1} = 1.0, k_1 = 0.965$ $\beta_{s1} = 1.0, k_1 = 0.675$
AC Fatigue Cracking	$\beta_{f1} = 0.02054, \beta_{f2} = 1.38, \beta_{f3} = 0.88$ $k_1 = 3.75, k_2 = 2.87, k_3 = 1.46$
Longitudinal Cracking	$C_1 = 7, C_2 = 3.5, C_4 = 1000$
Transverse Cracking	$\beta_{f3} = 0.88$

4.2 Assessment of the Total Rutting Prediction Model

The PMED software was used to calculate the total rut depths of selected LTPP asphalt pavement sections in Alabama, neighboring states, and the NCAT Test Track. These calculations were based on the critical inputs identified in Chapter 3. The predicted total rut depths were then compared with the corresponding field-measured rut depths. The comparison results, based on null

hypothesis tests, are summarized in Table 11 for three datasets: LTPP, LTPP_OL, and NCAT Test Track. The null hypothesis (H_0) of the statistical test (i.e., no significant difference existing between the predicted and measured data) was rejected for the conventional LTPP and Test Track datasets, indicating a significant bias in total rut depth prediction across these two datasets.

Table 11. Summary Statistics of the Globally Calibrated Rutting Model

Pavement Type	df	Bias	SEE	p -value	$H_0: \sum (Meas. - Pred.) = 0$
Test Track	479	0.165	0.202	<0.001	Rejected
LTPP	279	0.154	0.203	<0.001	Rejected
LTPP_OL	368	0.018	0.132	0.071	Not Rejected

Figure 18 provides a graphical comparison of the predicted and field-measured total rut depths. The total rut depth was notably over-predicted for the NCAT test track sections and, conversely, under-predicted for the conventional LTPP sections. The noticeable bias in the globally calibrated total rutting prediction model indicates that the model requires optimization for improved predictions.

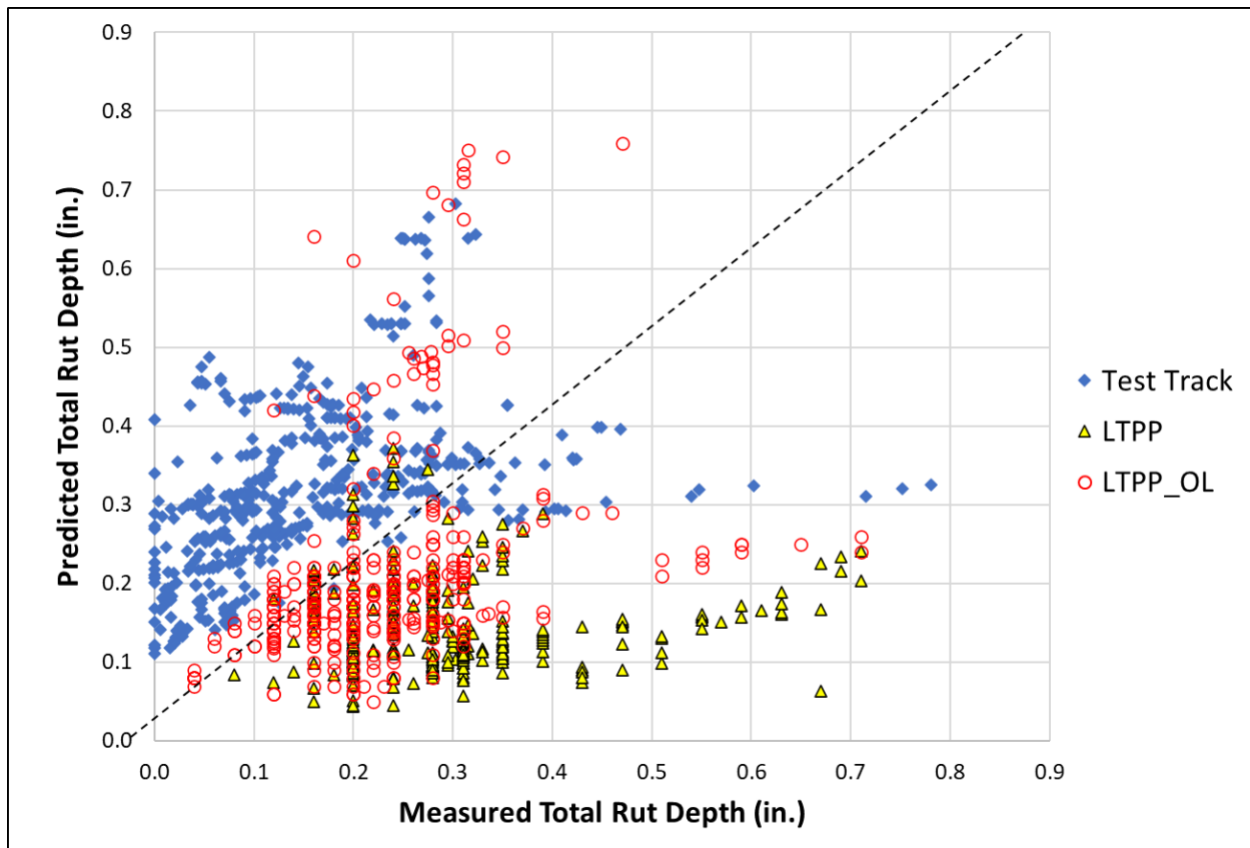


Figure 18. Comparison of Predicted and Measured Total Rut Depths

4.3 Assessment of the B-U Fatigue and Top-Down Cracking Models

The local verification of the globally calibrated bottom-up fatigue and longitudinal cracking prediction models used the same datasets that were used for the local verification of the rutting prediction model. In the MEPDG, bottom-up cracks start at the bottom of the asphalt layers and propagate to the surface, while longitudinal cracks initiate from the top and propagate downwards. The local verification results for the bottom-up fatigue cracking and longitudinal cracking models are summarized in Table 12 and Table 13, respectively. The statistical tests rejected the null hypothesis (H_0) for both models across all the datasets, indicating bias in the bottom-up fatigue and top-down cracking prediction models.

Table 12. Summary Statistics of the Globally Calibrated Bottom-Up Fatigue Cracking Model

Pavement Type	df	Bias	SEE	p-value	$H_0: \sum (Meas. - Pred.) = 0$
Test Track	441	2.938	14.03	<0.001	Rejected
LTPP	286	7.934	14.05	<0.001	Rejected
LTPP_OL	365	3.222	11.03	<0.001	Rejected

Table 13. Summary Statistics of the Globally Calibrated Top-Down Cracking Model

Pavement Type	df	Bias	SEE	p-value	$H_0: \sum (Meas. - Pred.) = 0$
LTPP	286	0.974	4.608	<0.001	Rejected
LTPP_OL	365	0.801	2.579	<0.001	Rejected

Figure 19 and Figure 20 present a comparison between the predicted and measured bottom-up fatigue and top-down cracking for the Test track, LTPP, and LTPP_OL sections. In Figure 19, there is a noticeable difference between the predicted and measured bottom-up fatigue cracking across the three datasets. For the Test Track sections, the blue diamonds are spread out, indicating that the PMED software may have either overpredicted or underpredicted the fatigue cracking percentages. The LTPP data, shown as yellow triangles, is mostly clustered near the x-axis, suggesting that the PMED software underpredicted the fatigue cracking percentages. The red circles, representing LTPP_OL data, were clustered on both sides of the line of equality at lower measured fatigue cracking values but became more dispersed as the measured fatigue cracking increased. This indicates the need for model optimization and further investigation to understand the differences across the datasets.

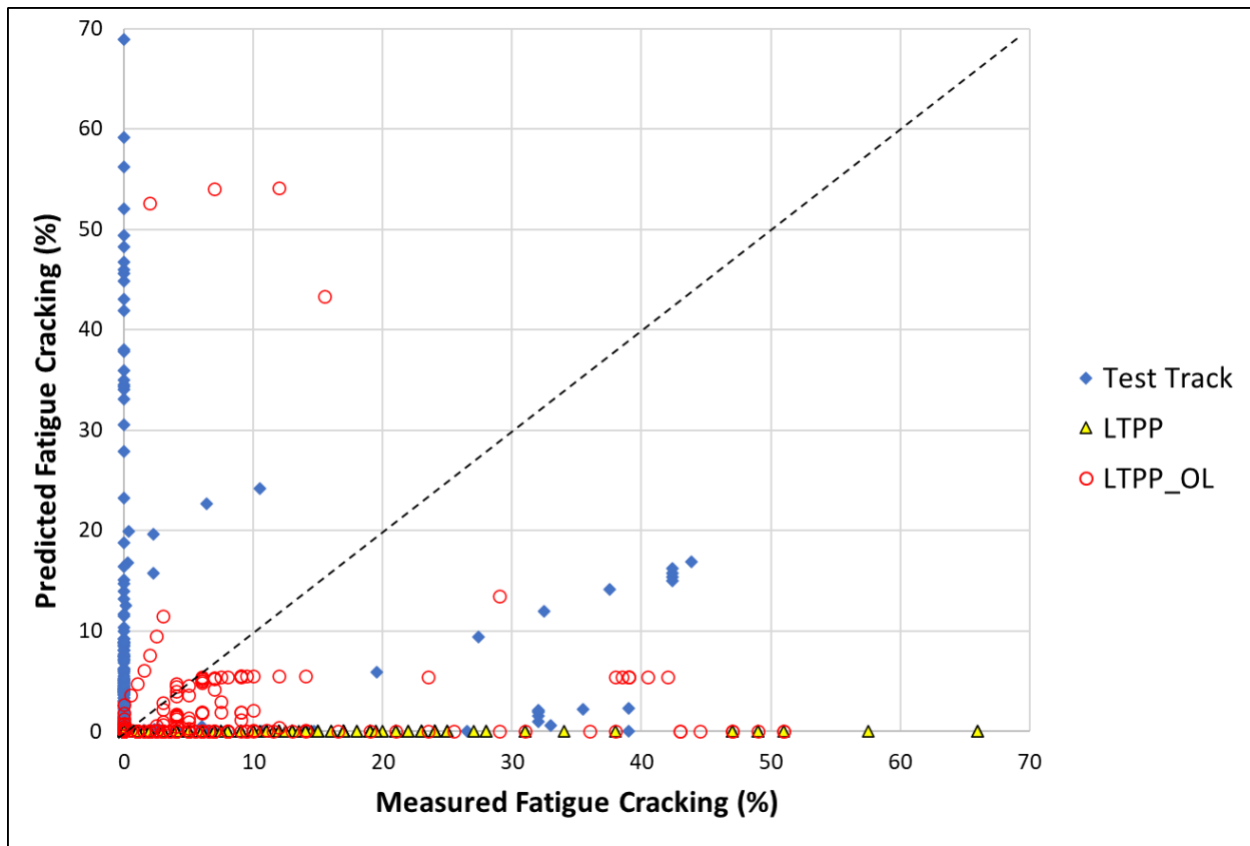


Figure 19. Comparison of Predicted and Measured Bottom-Up Fatigue Cracking

In Figure 21, most of the data points for both datasets are clustered near the lower left corner of the plot, indicating low values for both measured and predicted top-down cracking. There are fewer data points representing higher measured top-down cracking values. For the LTPP data, the yellow triangles are located along the x-axis, suggesting that they were underpredicted by the PMED software. On the other hand, the LTPP_OL data, represented by red circles, cluster at low measured and predicted cracking values on both axes, indicating both overprediction and underprediction. This suggests the need to recalibrate the model.

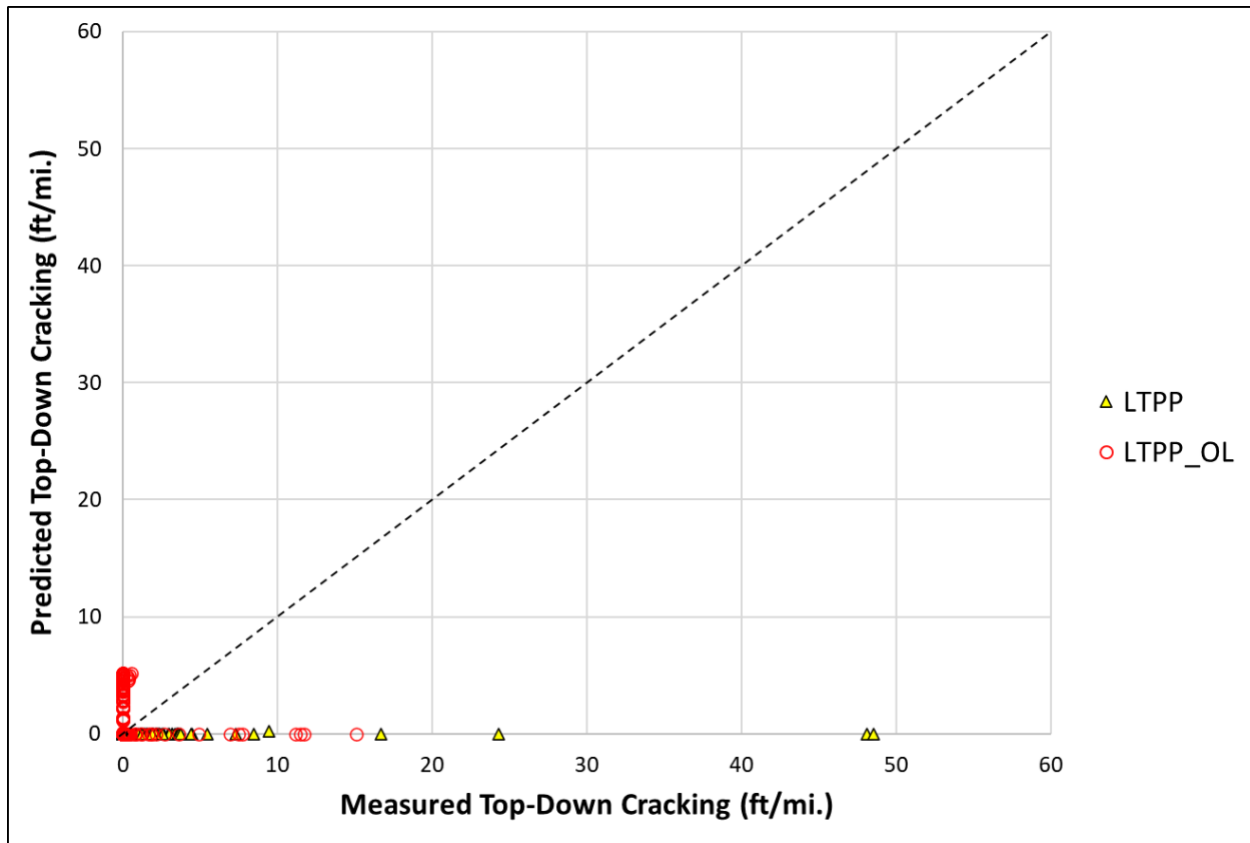


Figure 20. Comparison of Predicted and Measured Top-Down Cracking

4.4 Assessment of the Transverse Cracking Model

The globally calibrated transverse (or thermal) cracking prediction model was assessed using the LTPP and LTPP_OL datasets as data for transverse cracking in the Test Track sections were not available. The LTPP_OL data includes transverse and reflective cracking from the existing asphalt layer to the HMA overlays. Furthermore, the predicted transverse cracking in the PMED software is capped at 2112 ft/mi.

Table 14 summarizes the local verification results of the transverse cracking prediction model. The null hypothesis was rejected for both the LTPP and LTPP_OL datasets. Additionally, as illustrated in Figure 21, the model tends to overpredict. If ALDOT chooses to consider transverse cracking in the pavement design, the model needs to be recalibrated for local conditions.

Table 14. Summary Statistics of the Globally Calibrated Transverse Cracking Model

Pavement Type	df	Bias	SEE	p-value	$H_0: \sum (Meas. - Pred.) = 0$
LTPP	268	1165.04	1370	<0.001	Rejected
LTPP_OL	324	802.82	1132	<0.001	Rejected

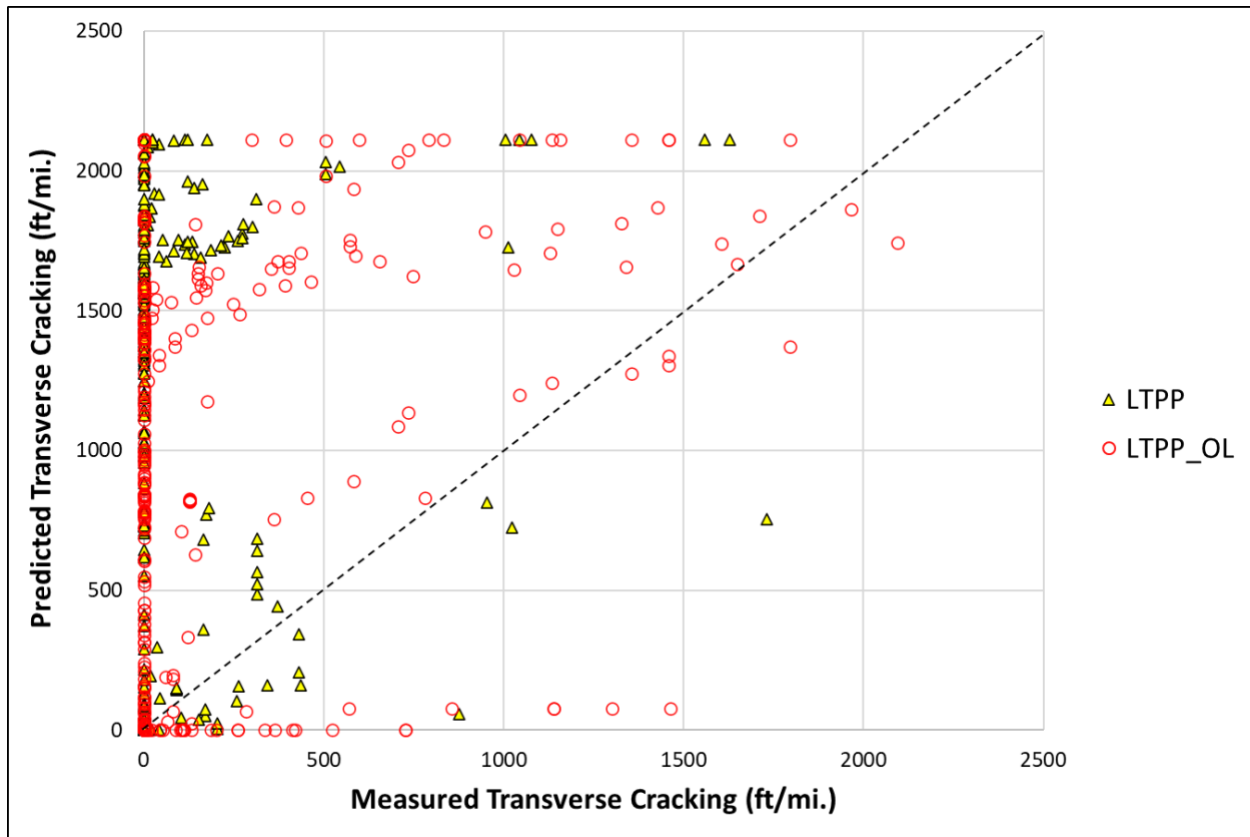


Figure 21. Comparison of Predicted and Measured Transverse Cracking

4.5 Assessment of the IRI Prediction Model

The IRI prediction model is a regression model that takes into account initial IRI, rutting, fatigue cracking, transverse cracking, and existing site conditions. The local verification results of the IRI prediction model are summarized in Table 15. The null hypothesis was rejected for the three datasets, indicating that a local calibration is needed. It is important to note that the IRI prediction model should only be optimized after the prediction models for rutting and cracking have been locally calibrated.

Table 15. Summary Statistics of the Globally Calibrated IRI Model

Pavement Type	df	Bias	SEE	p-value	$H_0: \sum (Meas. - Pred.) = 0$
Test Track	446	17.25	28.82	<0.001	Rejected
LTPP	267	15.18	18.86	<0.001	Rejected
LTPP_OL	344	19.64	24.63	<0.001	Rejected

Figure 22 shows the predicted and measured IRI for the three datasets. Most data points cluster above the line of equality, indicating that predicted IRI values tend to be higher than the measured values. The Test Track data, represented by blue diamonds, are more dispersed than the other two datasets. The significant spread and bias in the plot suggest that the IRI prediction model may need local calibration to improve its accuracy.

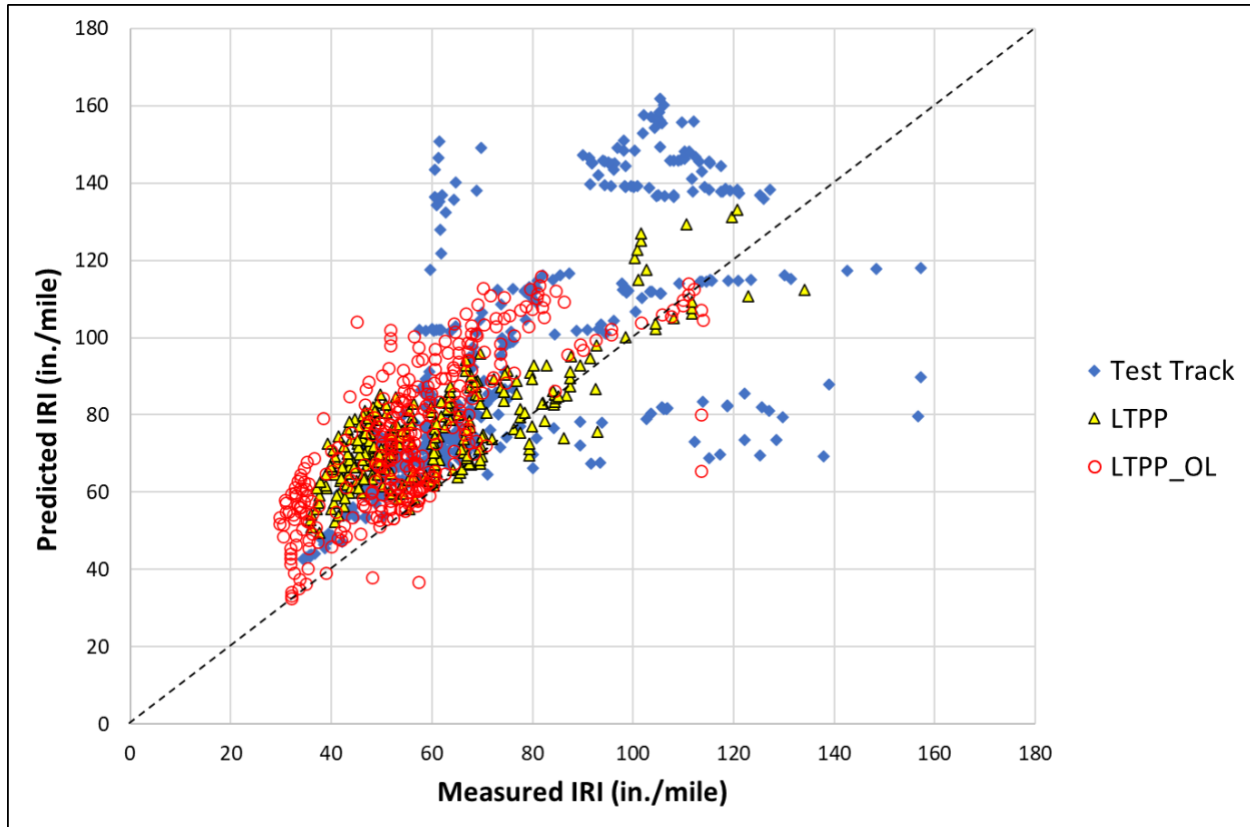


Figure 22. Comparison of Predicted and Measured IRI

CHAPTER 5 SUMMARY AND CONCLUSIONS

This research project aimed to conduct a local verification to assess the accuracy of globally calibrated Pavement ME Design distress and smoothness models for asphalt pavements in Alabama. The pavement sections used in this local verification included LTPP flexible pavement test sections in Alabama and neighboring states close to Alabama's state line, as well as structural pavement sections tested at the NCAT Test Track.

The study followed a rigorous local verification procedure, which involved selecting hierarchical input levels for each PMED input, choosing appropriate test sections, extracting and evaluating distress and project data, and assessing local bias and the standard error of the estimate. Data were sourced from the LTPP and NCAT Test Track databases, covering traffic inputs, pavement structures, climatic conditions, and field performance data.

Local verification results showed significant bias in the globally calibrated rutting prediction model when predicting rut depths for both general LTPP pavement sections and NCAT Test Track pavement sections. Both bottom-up and top-down cracking prediction models also exhibited bias across all datasets, with the PMED software underpredicting fatigue cracking percentages for general LTPP pavement sections and overpredicting fatigue cracking percentages for NCAT Test Track pavement sections. The transverse cracking model overpredicted transverse cracking for both LTPP and LTPP_OL datasets. Furthermore, the International Roughness Index prediction model showed a significant spread and bias, indicating higher predicted values than measured values.

Based on these key findings, local calibration of the PMED performance models is the next step in providing accurate predictions under Alabama conditions. In addition, the future implementation plan may also involve local validation with independent datasets and training on Pavement M-E Design.

In summary, the project demonstrated the importance of local verification of the prediction accuracy of pavement performance models. The findings suggest local calibration of Pavement ME Design is needed to improve its prediction accuracy, ensuring more reliable and cost-effective pavement structures.

REFERENCES

- AASHTO. (1986). *Guide for Design of Pavement Structures*. Washington, D.C.
- AASHTO. (1993). *Guide for Design of Pavement Structures*. Washington, D.C.
- AASHTO. (2010). *Guide for the Local Calibration of the Mechanistic-Empirical Pavement Design Guide*, American Association of State Highway and Transportation Officials, Washington, D.C.
- AASHTO. (2020). *Mechanistic-Empirical Pavement Design Guide; A Manual of Practice. Third Edition*, Washington D.C., 2020.
- AASHTO. AASHTO Interim Guide for Design of Pavement Structures. Washington, D.C., 1972.
- Bayomy, F., Muftah, A., Kassem, E., Tousef, F., and Alkuime, H. (2018). Calibration of the AASHTOWare Pavement ME Design Performance Models for Flexible Pavements in Idaho. Report No. FHWA-ID-18-235, Moscow, Idaho.
- Darter, M.I., Mallela, J., Titus-Glover, L., Rao, C., Larson, G., Gotlif, A., Von Quintus, H.L., et al. (2006). *NCHRP Research Results Digest 308: Changes to the Mechanistic–Empirical Pavement Design Guide Software Through Version 0.900, July 2006*. Transportation Research Board of the National Academies, Washington, DC.
- Darter, M.I., Titus-Glover, L., Von Quintus, H., Bhattacharya, B.B., & Jagannath, M. (2014). Calibration and Implementation of the AASHTO Mechanistic-Empirical Pavement Design Guide in Arizona. Arizona Department of Transportation, (FHWA-AZ-14-606). Retrieved from http://apps.azdot.gov/ADOTLibrary/Publications/project_reports/PDF/AZ606.pdf
- Federal Highway Administration (2013).
https://www.fhwa.dot.gov/policyinformation/tmguidetmg_2013/vehicle-types.cfm
- Gong, H., Huang, B., Shu, X., and Udeh, S. (2017). Experience with Local Calibration of the Mechanistic-Empirical Pavement Design Guide for Tennessee. *Road Materials and Pavement Design*, 18(sup 3): 130-138.
- HRB. The AASHO Road Test. Report 7, Summary Report, Highway Research Board. Report 61G, Washington D.C., 1962.
- Huilgol, P. (2020). Bias and Variance in Machine Learning – A Fantastic Guide for Beginners. <https://www.analyticsvidhya.com/blog/2020/08/bias-and-variance-tradeoff-machine-learning/>
- Kim, Y. R., Jadoun, F. M., Hou, T., and Muthadi, N. (2011a). “Local calibration of the MEPDG for flexible pavement design,” No. FHWA\NC\2007-07, North Carolina Department of Transportation Research and Analysis Group, North Carolina Department of Transportation, Raleigh, North Carolina.


- Kim, Y. R., Underwood, B., Far, M. S., Jackson, N., Puccinelli, J., & Engineers, N. C. (2011b). *LTPP computed parameter: dynamic modulus* (No. FHWA-HRT-10-035). United States. Federal Highway Administration.
- Prozzi, J. A., & Hong, F. (2006). Traffic Characterization for a Mechanistic-Empirical Pavement Design. Texas Department of Transportation Research and Technology Implementation Office, 7(22), 160.
- Robbins, M., Rodezno, C., Tran, N., and Timm, D. (2017). Pavement ME Design – A Summary of Local Calibration Efforts for Flexible Pavements. NCAT Report 17-07, Auburn, Alabama.
- Shuvo Islam. (2019). Implementation of AASHTOWare Pavement ME Design Software for Pavement Rehabilitation. Kansas State University, Manhattan, Kansas.
- Timm, D. (2009). *Design, Construction, and Instrumentation of the 2006 Test Track Structural Study*. Report No. 09-01, National Center for Asphalt Technology, Auburn University, 2009.
- Timm, D.H. and R. E. Turochy (2011). Introduction to Mechanistic-Empirical (M-E) Design Short Course. ALDOT Project 930-792, Alabama Department of Transportation. <http://www.eng.auburn.edu/files/centers/hrc/930-685.pdf>
- Timm, D.H., R. E. Turochy and K.P. Davis (2010). Guidance for M-E Pavement Design Implementation. ALDOT Project 930-685, Alabama Department of Transportation. <http://www.eng.auburn.edu/files/centers/hrc/930-685.pdf>
- Turochy, R.E., D.H. Timm and M.S. Tisdale (2005). Truck Equivalency Factors, Load Spectra Modeling and Effects on Pavement Design, Report No. 930-564, Submitted to Alabama Department of Transportation, Montgomery, AL. <http://www.eng.auburn.edu/files/centers/hrc/930-564.pdf>
- Von Quintus, H., Darter, M., Bhattacharya, B., and Titus-Glover, L. (2014). Calibration of the MEPDG Transfer Functions in Georgia. Report No. FHWA/GA-014-11-17, Champaign, Illinois.
- Von Quintus, H., Rao, C., Bhattacharya, B. (2017). Implementation and Preliminary Local Calibration of Pavement ME Design in Mississippi. Report No. FHWA/MS-DOT-RD-017-284, Champaign, Illinois.
- Von Quintus, H.L. and Moulthrop, J.S. (2007). *Mechanistic–Empirical Pavement Design Guide Flexible Pavement Performance Prediction Models for Montana: Volume II Reference Manual, Report No. FHWA/MT-07-008/8158-2*, Fugro Consultants, Inc.- Montana Department of Transportation, Austin, TX.
- Zhou, C., Huang, B., Shu, X., and Dong, Q. (2013). Validating MEPDG with Tennessee Pavement Performance Data. Journal of Transportation Engineering, 139(3): 306-312.
- JMP Statistical Discovery. (2023). https://www.jmp.com/en_us/statistics-knowledge-portal/what-is-regression/the-method-of-least-squares.html

APPENDICES

Appendix A - LTPP Data Extraction Procedure

- Log in to <https://infopave.fhwa.dot.gov/>
- Click on the Data tab.
- On the left-hand side of the Data page, click on Section which is a subsection of “General.”
- Select the pavement test section of interest.
- After selecting the pavement test section, click on “Pavement Structure and Construction” to expand the tab.
- Click on “General Section Information” to select all the data embedded in the subsection.
- Click on “Pavement Layer Type and Thickness” and select the embedded data.
- Click on “Material – Layer Properties and Field Sampling.” This subsection contains data of both flexible and rigid pavements. Select the data that applies to the pavement test section under consideration.
- Next is “Feature – Drainage, Joints, Shoulder, Reinforcement” subsection. This subsection can be ignored if the test section is a flexible pavement.
- Click on “Maintenance and Rehabilitation (M&R) subsection and select the data that applies to the pavement test section under consideration.
- Click on “Add to Selection” at the bottom of the “Pavement Structure and Construction” tab.
- Collapse the “Pavement Structure and Construction” tab and click on the “Traffic” tab.
- After expanding the “Traffic” tab, click on the “Inputs for AASHTOWare Pavement ME Design” and “Annual Traffic Inputs Over Time” subsections and select all the embedded data.
- Click on “Add to Selection” at the bottom of the “Traffic” tab.
- Collapse the “Traffic” tab and click on the “Performance” tab.
- Click on “Pavement Distress” to select pavement distress data that applies to the selected pavement test section.
- Click on “Surface Characteristics” and select the data that applies to selected test section.
- Click on “Backcalculation and Deflection” and select the data embedded in the “Backcalculation” subsection.
- Click on “Add to Selection” at the bottom of the “Performance” tab.
- Collapse the “Performance” tab and click on the “Add to Data Bucket” tab at the bottom of the page.
- Click on the “Go to Data Bucket” tab at the bottom of the page.
- Input your email address and preferred file format (i.e. .xlsx, .mdb, or .bak).
- Under the Unit System, click on US customary.
- Enter the CAPTCHA code provided and click on “Submit for Data Extraction” at the bottom of the page.

Appendix B - ANNACAP

 Input

Done

Input Parameters

Layer ID

State Code

01

Project ID

4127

Project Layer

6

Construction Date

08-Aug-89

Choose

Aging Level

RTFO/TFO

Model

Model to Use

Viscosity Based ANN

Analysis Level

Level 3

VMA

15

9.51% - 34.64%

VFA

75

32.82% - 95.07%

Binder Grade

AC-20

A

10.7709

VTs

-3.6017

STATE_C ODE	PROJECT _ID	PROJECT_L AYER	CONSTRUCTION _DATE	SAMPLE_T YPE	PREDICTIVE_M ODEL	TEMPERATURE_(DEG_F)	FREQUENCY _(HZ)	E* _PREDICTIO N_(PSI)
1	4127	6	8-Jun-89	2	VV-Grade	14	25.0	4,392,665
1	4127	6	8-Jun-89	2	VV-Grade	14	10.0	4,304,568
1	4127	6	8-Jun-89	2	VV-Grade	14	5.0	4,198,818
1	4127	6	8-Jun-89	2	VV-Grade	14	1.0	3,842,762
1	4127	6	8-Jun-89	2	VV-Grade	14	0.5	3,688,187
1	4127	6	8-Jun-89	2	VV-Grade	14	0.1	3,177,665
1	4127	6	8-Jun-89	2	VV-Grade	40	25.0	3,983,040
1	4127	6	8-Jun-89	2	VV-Grade	40	10.0	3,883,345
1	4127	6	8-Jun-89	2	VV-Grade	40	5.0	3,770,269
1	4127	6	8-Jun-89	2	VV-Grade	40	1.0	3,403,650
1	4127	6	8-Jun-89	2	VV-Grade	40	0.5	3,230,691
1	4127	6	8-Jun-89	2	VV-Grade	40	0.1	2,609,466
1	4127	6	8-Jun-89	2	VV-Grade	70	25.0	1,809,784
1	4127	6	8-Jun-89	2	VV-Grade	70	10.0	1,616,601
1	4127	6	8-Jun-89	2	VV-Grade	70	5.0	1,451,864
1	4127	6	8-Jun-89	2	VV-Grade	70	1.0	1,034,180
1	4127	6	8-Jun-89	2	VV-Grade	70	0.5	891,588
1	4127	6	8-Jun-89	2	VV-Grade	70	0.1	538,907
1	4127	6	8-Jun-89	2	VV-Grade	100	25.0	578,941
1	4127	6	8-Jun-89	2	VV-Grade	100	10.0	449,981
1	4127	6	8-Jun-89	2	VV-Grade	100	5.0	368,697
1	4127	6	8-Jun-89	2	VV-Grade	100	1.0	214,226
1	4127	6	8-Jun-89	2	VV-Grade	100	0.5	173,263
1	4127	6	8-Jun-89	2	VV-Grade	100	0.1	91,549
1	4127	6	8-Jun-89	2	VV-Grade	130	25.0	165,589
1	4127	6	8-Jun-89	2	VV-Grade	130	10.0	127,403
1	4127	6	8-Jun-89	2	VV-Grade	130	5.0	102,585
1	4127	6	8-Jun-89	2	VV-Grade	130	1.0	57,817

1	4127	6	8-Jun-89	2	VV-Grade	130	0.5	47,796
1	4127	6	8-Jun-89	2	VV-Grade	130	0.1	29,758